© 2005 Elsevier B.V. All rights reserved.
Theory and Applications of Computational Chemistry: The First Forty Years
Edited by C. Dykstra et al.

CHAPTER 10

Finding minima, transition states, and following reaction pathways on ab initio *potential energy surfaces*

Hrant P. Hratchian and H. Bernhard Schlegel

Department of Chemistry and Institute for Scientific Computing, Wayne State University, Detroit, MI 48202, USA

Abstract

Potential energy surfaces (PESs) form a central concept in the theoretical description of molecular structures, properties, and reactivities. In this chapter, recent advancements and commonly used techniques for exploring PESs are surveyed in the context of electronic structure methods. Specifically, minimization, transition state optimization, and reaction path following are discussed. In addition to reviewing current progress in these areas, this chapter offers a number of practical discussions regarding minimization, transition state optimization, and reaction path following, including suggestions for overcoming common pitfalls.

10.1 INTRODUCTION

Potential energy surfaces (PESs) play a central role in computational chemistry. The study of most chemical processes and properties by computational chemists begins with the optimization of one or more structures to find minima on PESs, which correspond to equilibrium geometries. To obtain reaction barriers and to calculate reaction rates using transition state theory (TST) [1,2], it is necessary to locate first-order saddle points on the PES, which correspond to transition states (TS). Often one needs to confirm that a TS lies on a pathway that actually connects the minima corresponding to reactants and products (i.e. a TS that is involved in the chemical process under investigation). This goal is typically accomplished by following the steepest descent reaction pathway downhill in each direction from the TS to the reactant minimum and to the product minimum. The reaction path can also be used in the computation of reaction rates using more

References pp. 243–249

sophisticated models such as variational transition state theory (VTST) and reaction path Hamiltonians (RPH) [3–7].

In this chapter, standard algorithms for these calculations—minimization, TS optimization, and reaction path following—are discussed. It should be noted that a number of reviews on these and related methods have appeared in the literature [8–24], including an excellent book on PESs and methods for exploring their landscapes by Wales [25]. Although an exhaustive review of the methods available to computational chemists would be of historical value, our presentation here, heeding to space limitations and a desire to maintain readability, focuses on algorithms commonly used in studies presented in the current literature. Nevertheless, approaches that are less often used in modern practice are included where they provide a map of methodology evolution and are pedagogically useful.

In the next section, essential background material is provided. In Section 10.3, methods for minimization are discussed followed by TS optimization methods in Section 10.4. Reaction path following is considered in Section 10.5. In Section 10.6, we conclude by summarizing the current state of this active area of research.

10.2 BACKGROUND

In this section, concepts that are common to multiple topics and those that form the foundation for the methods and algorithms presented here are discussed. We begin by developing the PES construct from the Born–Oppenheimer (BO) approximation. Next, we discuss the computation of analytic PES derivatives in the context of quantum chemical calculations. In the last part of this section, we consider the common coordinate systems used in optimization and reaction path following.

10.2.1 Potential energy surfaces

The PES arises naturally upon application of the BO approximation to the solution of the Schrödinger equation. We begin by considering the general Hamiltonian

$$H = T_r + T_R + V(r, R) \tag{1}$$

where T_r is the operator for the kinetic energy of electronic motion, T_R is the operator for the kinetic energy of nuclear motion, and $V(r, R)$ is the potential energy due to electrostatic interactions between all of the charged particles (electrons and nuclei). The BO approximation is applied by assuming that the three order of magnitude difference in the mass of nuclei and electrons renders the nuclei fixed in space on the time scale of electron motion. As a result, the nuclear kinetic energy term, T_R, in the molecular Hamiltonian vanishes and the electronic and nuclear degrees of freedom can be separated. This yields the time-independent Schrödinger equation for the electronic degrees of freedom

$$[T_r + V(r, R)]\Phi(r; R) = E(R)\Phi(r; R) \tag{2}$$

In Eq. (2) $\Phi(r;R)$ is the electronic wavefunction, which depends parametrically on the nuclear positions, and the energy of the system, $E(R)$, is a function of the nuclear degrees of freedom. A plot of E *vs.* R gives the PES. For each non-degenerate electronic state, a different PES exists.

Fig. 10.1 shows a model PES. The potential energy of the system is given by the vertical axis and nuclear coordinates are given by the horizontal axes. A common analogy compares the topology of PESs to mountainous landscapes [26]. Molecular structures correspond to the positions of minima in the valleys. Reaction rates can be determined from the height and profile of the pathway connecting reactant and product valleys. Relative stabilities of isomers can be determined from the energies, or elevations, of the minima on the PES corresponding to each structure. From the shape of a valley, the vibrational spectrum of a molecule can be computed, and the response of the energy to electric and magnetic fields determines molecular properties such as dipole moment, polarizability, NMR shielding, etc. [8,27–29].

For simple systems, the PES can be fitted to experimental data. Molecular mechanics (MM) methods can also generate approximate PESs very quickly. However, the types of reactions that can be investigated using conventional MM methods are very limited. Thus, for more complex and reactive systems these options are not viable, and one must rely on PESs generated using quantum chemical calculations (i.e. semi-empirical, *ab initio*, density functional theory (DFT), etc.).

In this chapter, we will explore a number of methods designed to navigate through the mountain ranges of a PES to find local valleys (minimization), the highest point along a reaction path through a mountain pass connecting reactant and product valleys (TS optimization), and the path of least resistance down from the mountain pass to the valleys below (reaction path following). In general, we are concerned with reactive systems, i.e. chemistries involving bond making and breaking that cannot be treated using

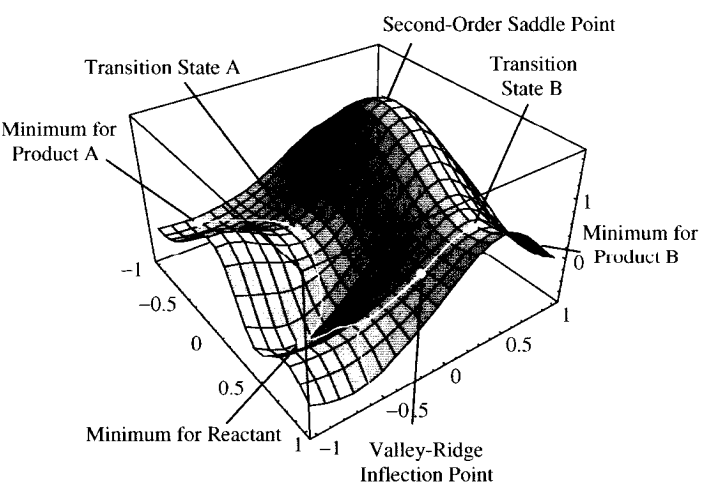

Fig. 10.1. Model potential energy surface showing minima, transition states, a second-order saddle point, reaction paths, and a valley ridge inflection point (from Ref. [72] with permission).

conventional MM methods. Therefore, the focus here is on PESs determined using quantum chemical calculations. Additionally, minimization algorithms designed specifically for use with hybrid quantum mechanical/molecular mechanics (QM/MM) methods are included.

10.2.2 Analytic PES derivatives

One point that is not always obvious after one's first encounter with the BO approximation is that the PES is not known *a priori*. As discussed above, one may fit a functional form to experimental and/or high-level quantum chemical calculation data, but in most applications of electronic structure methods this is not practical. All of the methodologies discussed in this chapter were designed with this in mind. When an algorithm is used to navigate a PES, the value of the energy at each new point is unknown and must be calculated.

Going back to the mountain range analogy [26], we can think of the starting structure supplied by the user for a minimization, TS optimization, or reaction path following calculation as a hiker who is dropped somewhere in the middle of the mountain range. The hiker's latitude and longitude correspond to the molecule's geometry and the elevation corresponds to the value of the PES. Depending on the type of calculation, we may want the hiker to head to the bottom of a valley (minimization), to the top of a mountain pass (TS optimization), or to follow the steepest pathway downhill from the top of a mountain pass to a valley floor (reaction path following). Since the global PES is not known, our hiker is essentially blind. Quantum chemical calculations provide the navigation tools. Energy calculations can be thought of as an altimeter, giving the current elevation. For the hiker to know the slope of the landscape, we also need to calculate the first derivatives of the energy with respect to the nuclear coordinates, or gradients. Note that the negative of the gradient on the PES is equal to the force. As a result, the terms 'gradient' and 'force' are often used interchangeably. If we compute the second derivatives of the energy with respect to the nuclear coordinates, or Hessian, the hiker now knows about the local curvature of the mountain range. The Hessian gives the force constants of the harmonic vibrations of the molecule, and is therefore often referred to as the 'force constant matrix.'

Although the hiker would certainly like as much help as possible, we must consider the relative cost of energy and derivative calculations and the usefulness of each computation. There is a definite trade-off involved between information and expense. To illustrate this point, let us consider minimization. The user's initial guess at the geometry of the structure places our hiker somewhere in the PES mountain range. Calculating the energy alone at this initial position does not provide the hiker with enough information to begin stepping toward the valley floor. Calculating the gradient, though, tells the hiker which direction is downhill. Now, the hiker can take a step towards the bottom of the valley. However, the optimal size of the step is not known. As a result, if too large a step is taken the hiker may overshoot the minimum and go to the other side of the valley. Or worse, the hiker may step through a mountain to a point in a different valley altogether! If the hiker is also given the force constants, the local quadratic

character of the mountain range is known. Combined with the gradient, the hiker can take larger steps with greater confidence using the Hessian. Of course, in some applications the cost of the Hessian may be more than what we are willing to pay for the hiker's ability to take larger steps.

To discuss the form and cost of analytic gradient and Hessian evaluations, we consider the simple case of Hartree–Fock (HF) calculations. In nearly all chemical applications of HF theory, the molecular orbitals (MOs) are represented by a linear combination of atomic orbitals (LCAO). In the context of most electronic structure methods, the LCAO approximation employs a more convenient set of basis functions such as contracted Gaussians, rather than using actual atomic orbitals. Taken together, the collection of basis functions used to represent the atomic orbitals comprises a basis set.

Within the LCAO approximation, the HF energy for a spin restricted, closed shell system is given by

$$\begin{aligned} E &= \langle \Phi | H | \Phi \rangle \\ &= 2\sum_i (\phi_i | H_1 | \phi_i) + \sum_{ij} \left[2\left(\phi_i \phi_j \middle| \frac{1}{r} \middle| \phi_i \phi_j\right) - \left(\phi_i \phi_j \middle| \frac{1}{r} \middle| \phi_j \phi_i\right) \right] + V_{NN} \\ &= \sum_{\mu\nu} (\mu | H_1 | \nu) P_{\mu\nu} + \frac{1}{2} \sum_{\mu\nu\lambda\sigma} (\mu\nu|\lambda\sigma)(P_{\mu\nu}P_{\lambda\sigma} - \frac{1}{2} P_{\mu\sigma}P_{\lambda\nu}) + V_{NN} \end{aligned} \tag{3}$$

where Φ is the electronic wavefunction, H is the Hamiltonian, $\phi_i = \Sigma c_{\mu i}\chi_\mu$ are the MOs expanded as a linear combination of basis functions χ, H_1 is the one-electron Hamiltonian (kinetic energy and nuclear-electron attraction), $(\mu\nu|\lambda\sigma)$ are the electron–electron repulsion integrals, μ, ν, λ and σ denote the basis functions, and $\mathbf{P}$ is the density matrix given by

$$\mathbf{P}_{\mu\nu} = 2 \sum_{i=1}^{\text{occupied}} c_{\mu i}^* c_{\nu i} \tag{4}$$

where the summation is over occupied MOs and the factor of two comes from the fact that each occupied MO holds two electrons. Formally, calculation of the HF energy is $\mathcal{O}(N_{\text{basis}}^4)$ computational work, where N_{basis} is the number of basis functions. Density functional methods are comparable in cost to HF and a number of developments have been made recently to achieve linear and near-linear scaling for large systems [30–38].

The first derivative of the energy with respect to a nuclear coordinate, q_i, (i.e. the gradient) is given by

$$\frac{\partial E}{\partial q_i} = \left\langle \Phi \middle| \frac{\partial H}{\partial q_i} \middle| \Phi \right\rangle + 2\left\langle \frac{\partial \Phi}{\partial q_i} \middle| H \middle| \Phi \right\rangle \tag{5}$$

The first term in Eq. (5) is the Hellman–Feynman term and the second term is the wavefunction derivative, or Pulay, term. The Hellman–Feynman portion of the gradient involves a basic computation of the expectation value of a one electron operator. The wavefunction derivative term, which arises because atom-centered basis functions are used, depends on the derivatives of the one- and two-electron integrals in Eq. (3).

Expanding Eq. (5) into a more convenient form for quantum chemical calculations gives

$$\frac{dE}{dq_i} = 2\sum_{\mu\nu} \frac{d(\mu|H_1|\nu)}{dq_i} P_{\mu\nu} + \sum_{\mu\nu\lambda\sigma} \frac{d(\mu\nu|\lambda\sigma)}{dq_i} (2P_{\mu\nu}P_{\lambda\sigma} - P_{\mu\lambda}P_{\nu\sigma}) - 2\sum_{\mu\nu} \frac{dS_{\mu\nu}}{dq_i} W_{\mu\nu} \quad (6)$$

where $S_{\mu\nu}$ are the overlap matrix elements and

$$\mathbf{W} = \mathbf{PFP} \quad (7)$$

where **F** is the Fock matrix. In terms of the basis functions, the elements of the Fock matrix are given by

$$F_{\mu\nu} = 2\sum_{\mu\nu} (\mu|H_1|\nu) P_{\mu\nu} + \sum_{\mu\nu\lambda\sigma} (\mu\nu|\lambda\sigma)(2P_{\mu\nu}P_{\lambda\sigma} - P_{\mu\sigma}P_{\lambda\nu}) \quad (8)$$

This form for the gradient was introduced by Pulay in 1969 [39], and it serves as the basis for the subsequent development of analytic energy derivatives for many different theoretical levels, including correlated methods [28]. The computational cost of the HF gradient calculation is formally $\mathcal{O}(N_{\text{basis}}^4)$. Linear scaling methods have also been developed [32,33,37]. The cost of an analytic gradient evaluation is roughly the same as for the energy calculation. Thus, analytic gradient calculations are relatively routine for *ab initio* PESs and do not generally represent a cost barrier for calculations.

Hessian calculations, on the other hand, are much more expensive and their use in PES exploration methods adds appreciable cost to the calculations. Therefore, as we will show in the later sections of this chapter, estimated and updated Hessians are often used where second derivatives are required by the equations directing movement on the PES. For some systems, the assumptions used to estimate the Hessian are not valid. In these cases, or for cases where very accurate force constants are necessary for vibrational energy calculations, computed (either numeric or analytic) Hessians may be necessary.

Prior to 1979, analytic calculation of second derivatives for *ab initio* methods was thought to be unreasonably expensive [40]. However, in that year Pople et al. [41] developed an efficient approach to solve the coupled perturbed HF (CPHF) equations making analytic Hessian calculation very practical. Indeed, analytic computation of the Hessian is generally cheaper than numeric evaluation of second derivatives and the calculation of *ab initio* force constants by analytic methods is typical for systems with a few hundred basis functions on commercially available computers. Analytic Hessians are routinely available in electronic structure programs for semi-empirical, HF, DFT, second-order Møller-Plesset (MP2), complete active space self-consistent field (CASSCF), configuration interaction singles (CIS), and for other levels of theory. Solution of the CPHF equations for force constants can be expanded to solve for third and higher order derivatives as well [42–47]. However, derivative calculations become increasingly expensive as the order is increased. Therefore, most PES exploration methods developed for use with moderate to large systems limit analytic derivative calculations to second order, and for large systems will often attempt to limit the number of analytic Hessian evaluations.

10.2.3 Coordinate systems

When defining the PES one can use a number of different coordinate systems to describe the geometry of the system being studied; the simplest of these being Cartesian coordinates. In Cartesian coordinate space, the position of each atom in the molecule (or cluster, etc.) is given by three spatial coordinates, x, y, and z. For a system having N_{atoms} atoms there will be a set of $3N_{\text{atoms}}$ Cartesian coordinates, $\{x_i\}$. A similar coordinate system, which naturally develops in the context of nuclear motion (i.e. molecular vibrations, reaction path following, molecular dynamics, etc.), is mass-weighted Cartesian coordinates, $\{\tilde{x}_i\}$, given by

$$\tilde{x}_i = x_i\sqrt{m_N} \tag{9}$$

where $\{m_N\}$ give the atomic masses. Note that the subscript i goes over all of the coordinates while the subscript N goes over the corresponding atomic centers.

An undesirable property of Cartesian coordinates (with or without mass-weighting) is that they generate PESs with strongly coupled coordinates. An alternative to the Cartesian coordinate systems is internal coordinates, sometimes referred to as Z-matrix coordinates. This set of coordinates defines the molecular structure in terms of bond lengths, angles, and dihedral angles. For a non-linear molecule, a unique structure is defined by $3N_{\text{atoms}} - 6$ internal coordinates; for a linear molecule $3N_{\text{atoms}} - 5$ internal coordinates are required. Because internal coordinates are based upon the connectivity of the molecule, they are very natural for chemical systems. Furthermore, nuclear motion on a PES defined in internal coordinates results in much weaker coupling between coordinates than when the PES is given in Cartesian coordinates.

It has been shown that adding some redundancy in the internal coordinates generates a more effective coordinate system, especially for cyclic molecules [48–52]. The molecule's geometry is described using all the chemically relevant bond lengths, angles, and dihedrals, often more than the minimal $3N_{\text{atoms}} - 5$ or $3N_{\text{atoms}} - 6$ internal coordinates needed to specify the structure. As a simple example, consider benzene. There are 12 atoms in benzene, which gives rise to 36 Cartesian coordinates and 30 internal coordinates. The number of redundant internal coordinates is 54—12 bonds, 18 angles, and 24 dihedrals. It should be noted that the number of redundant internal coordinates can be altered by using different degrees of redundancy, and a multitude of definitions have been proposed [49,50,52–55]. They all perform as well as or better than Cartesian and non-redundant internal coordinates.

Since the quantum chemical calculation of energy and derivatives is easiest in the Cartesian space, it is necessary to convert these values to, and from, internals. Although the transformation from Cartesian coordinates to internals (minimal or redundant) is straightforward for the positions, the transformation of Cartesian gradients and Hessians requires a generalized inverse of the transformation matrix [49] *viz.*

$$\Delta\mathbf{q} = \mathbf{B}\Delta\mathbf{x},\ \ \mathbf{g}_q = \mathbf{B}^{-1}\mathbf{g}_x,\ \ \mathbf{H}_q = \mathbf{B}^{-t}\left(\mathbf{H}_x - \frac{\partial\mathbf{B}}{\partial\mathbf{x}}\mathbf{g}_q\right)\mathbf{B}^{-1},\ \ \mathbf{B} = \frac{\partial\mathbf{q}}{\partial\mathbf{x}} \tag{10}$$

In Eq. (10) **q** are the internal coordinates, **x** are the Cartesian coordinates, **g** is the gradient, **H** is the Hessian, and the Wilson B matrix is given by **B**. Throughout this chapter, a superscript 't' denotes transpose. Finite displacements in redundant internal coordinates require that the back transformation of the positions to Cartesian coordinates be solved iteratively using Eq. (10) and

$$\mathbf{x}_1 = \mathbf{x}_0 + \mathbf{u}\mathbf{B}^t\mathbf{G}^{-1}\Delta\mathbf{q} \tag{11}$$

where

$$\mathbf{G} = \mathbf{B}\mathbf{u}\mathbf{B}^t \tag{12}$$

and **u** is an arbitrary matrix.

The calculation of the generalized inverses in Eqs. (10) and (11) scales as $\mathcal{O}(N_{\text{atoms}}^3)$. Although the cost for this calculation can become significant for large molecules, it is often the case that this cost is far outweighed by the cost of energy and derivative calculations. Nevertheless, for large systems and studies where a low level of theory is used (resulting in relatively fast energy and derivative calculations) the computation of the generalized inverse can become a bottleneck. To make the redundant internal ↔ Cartesian coordinate transformations more tractable, techniques such as iterative solutions to linear equations, Cholesky decomposition, and sparse matrix methods have been developed and reported in the recent literature [56–63]. Using these methods, the redundant internal ↔ Cartesian coordinate transformations can be achieved with linear scaling. The costs of coordinate transformations are more than compensated for by the increased efficiency of the optimization algorithms that use them by decreasing the number of steps required by the algorithm, which in turn decreases the number of energy and derivative evaluations required to complete the job.

10.3 MINIMIZATION

At the start of nearly all chemical studies using electronic structure methods, geometry optimization is required. In this section, we explore some of the most utilized algorithms for minimization. As stated earlier, our focus here is on methods developed for use with quantum chemical calculations where simple functions of the energy and derivatives of the PES are not available but rather are calculated by electronic structure methods as needed. It should also be kept in mind that compared to the cost of the energy calculation a geometry optimization step in most cases is inexpensive. Topics related to global optimization [13–17] and methods catered toward specific advantages or disadvantages of fitted and empirical PESs [11,64–67] are beyond the scope of this chapter.

The problem of geometry optimization involves an unconstrained minimization on the PES. The numerical analysis literature abounds with methods for minimizing non-linear functions of many variables [68–71]. These methods can be placed in three general categories: methods using only the energy, gradient based methods, and methods employing second derivatives. Although energy-only algorithms are applicable across the widest range of levels of theory and problems, they tend to be the least efficient and

require a large number of steps to converge. On the other hand, methods that use the Hessian are likely to converge in the least number of steps. However, as discussed in Section 10.2, Hessian evaluation can be quite costly and convergence in a small number of steps may not necessarily equate to the least expensive overall calculation. Gradient-based optimizers often give the best balance between the energy/derivative costs and rate of convergence. As a result, the most commonly used geometry minimization algorithms are gradient based.

Regardless of which method is used, all geometry minimizations are comprised of three basic elements. First, energy and derivatives are computed at the initial geometry. Second, the geometry is changed to take a step toward the minimum. Third, a test (or series of tests) is carried out to determine if the new position is close enough to the PES minimum. If it is, the minimization is complete. If not, the process is repeated to take another step toward the minimum.

Included in the methods discussed below are Newton-based methods (Section 10.3.1), the geometry optimization by direct inversion of the iterative subspace, or GDIIS, method (Section 10.3.2), QM/MM optimization techniques (Section 10.3.3), and algorithms designed to find surface intersections and points of closest approach (Section 10.3.4). We conclude the discussion of minimization methods in Section 10.3.5 with a discussion of practical considerations related to minimization, including suggestions for overcoming common problems.

10.3.1 Newton methods

It has been well established that Newton-based methods are the most efficient type for minimization problems [9,11,12,25,72]. The starting point for these algorithms is to approximate the PES by a Taylor series expansion about the current point, $\mathbf{x}_0$. Truncating the expansion at second order gives

$$E(\mathbf{x}) = E_0 + \mathbf{g}_0^t \Delta\mathbf{x} + \frac{1}{2}\Delta\mathbf{x}^t \mathbf{H}_0 \Delta\mathbf{x} \tag{13}$$

The gradient, $\mathbf{g}(\mathbf{x})$, for this Taylor series is

$$\mathbf{g}(\mathbf{x}) = \mathbf{g}_0 + \mathbf{H}_0 \Delta\mathbf{x} \tag{14}$$

In Eq. (13), E_0, $\mathbf{g}_0$, and $\mathbf{H}_0$ give the energy, gradient, and Hessian at the point $\mathbf{x}_0$ and

$$\Delta\mathbf{x} = \mathbf{x}_i - \mathbf{x}_0 \tag{15}$$

At the minimum, the gradient will be zero,

$$\mathbf{g}(\mathbf{x}) = \mathbf{g}_0 + \mathbf{H}_0 \Delta\mathbf{x} = 0 \tag{16}$$

Solving for $\Delta\mathbf{x}$ gives the step that leads to the minimum in the local quadratic region,

$$\Delta\mathbf{x} = -\mathbf{H}^{-1}\mathbf{g} \tag{17}$$

where the subscript '0' from (16) has been dropped for convenience. Eq. (17) is the Newton step, which is the basis of most minimization methods. Formally speaking, when analytic gradients and Hessians are both used to take steps according to Eq. (17) the algorithm is known as Newton–Raphson (NR). A general flowchart for Newton methods of optimization is shown in Fig. 10.2.

Since analytic Hessians can be rather expensive, especially for larger systems, it is advantageous to avoid computing second derivatives. Nevertheless, the NR algorithm is much more efficient than methods using only gradient or only energy information. The quasi-Newton (QN) approach satisfies both of these concerns. The QN step direction is still determined using Eq. (17), but instead of using an analytic Hessian at each step we begin with an approximate Hessian at the start of the calculation (i.e. an empirically estimated Hessian or a Hessian computed at a lower level of theory) and use Hessian updating at the subsequent steps in the optimization. Hessian updating approximates the Hessian using the change in position and gradient from the previous step. Commonly used updating schemes include Murtagh–Sargent (MS) or symmetric rank 1 (SR1), Powell symmetric Broyden (PSB), Davidson–Fletcher–Powell (DFP), and Broyden–Fletcher–Goldfarb–Shanno (BFGS) [68–71,73–78]. The BFGS update is generally

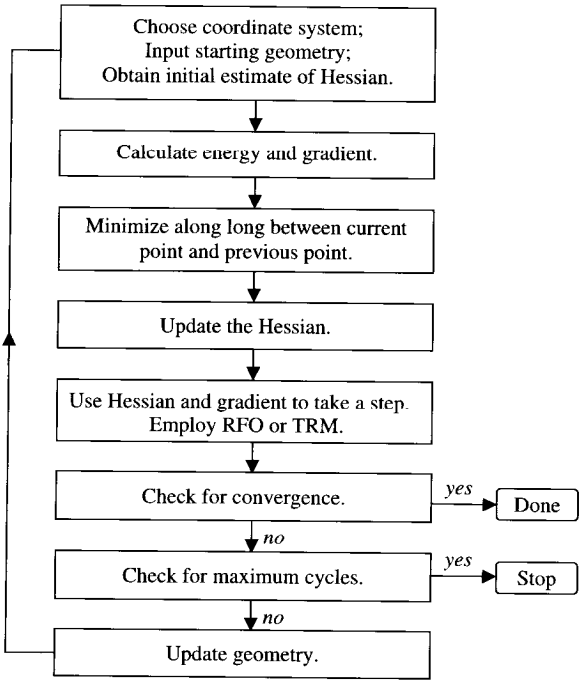

Fig. 10.2. Flowchart for quasi-Newton geometry optimization algorithms (from Ref. [72] with permission).

accepted as the best formula for minimizations and is given by

$$\mathbf{H}^{\text{new}} = \mathbf{H}^{\text{old}} + \frac{\Delta\mathbf{g}\Delta\mathbf{g}^{\text{t}}}{\Delta\mathbf{x}^{\text{t}}\Delta\mathbf{g}} - \frac{\mathbf{H}^{\text{old}}\Delta\mathbf{x}\Delta\mathbf{x}^{\text{t}}\mathbf{H}^{\text{old}}}{\Delta\mathbf{x}^{\text{t}}\mathbf{H}^{\text{old}}\Delta\mathbf{x}} \tag{18}$$

Eq. (18) is symmetric and positive definite (i.e. the eigenvalues of the Hessian are all positive), and minimizes the norm of the change in the Hessian. Corresponding updating formulae also exist for the inverse of the Hessian [68–71,77], which allow the algorithm to avoid the inversion of **H** needed in Eq. (17).

A modification to Bofill's update method (which was originally designed for use in TS optimizations) [79] is also very useful for minimization. This update combines the BFGS and MS schemes, and is given by

$$\mathbf{H}^{\text{new}} = \phi\Delta\mathbf{H}^{\text{BFGS}} + (1 - \phi)\Delta\mathbf{H}^{\text{MS}} \tag{19}$$

where the MS update is

$$\Delta\mathbf{H}^{\text{MS}} = \frac{(\Delta\mathbf{g} - \mathbf{H}^{\text{old}}\Delta\mathbf{x})(\Delta\mathbf{g} - \mathbf{H}^{\text{old}}\Delta\mathbf{x})^{\text{t}}}{\Delta\mathbf{x}^{\text{t}}(\Delta\mathbf{g} - \mathbf{H}^{\text{old}}\Delta\mathbf{x})} \tag{20}$$

and the coefficient is computed according to

$$\phi = \frac{|\Delta\mathbf{x}^{\text{t}}(\Delta\mathbf{g} - \mathbf{H}^{\text{old}}\Delta\mathbf{x})|}{|\Delta\mathbf{x}||\Delta\mathbf{g} - \mathbf{H}^{\text{old}}\Delta\mathbf{x}|} \tag{21}$$

Minimization of most small and moderately sized systems is handled very well by QN optimization. For more difficult cases, it is sometimes useful to calculate analytic Hessians at the beginning, every few steps, or even at every step, rather than using updated second derivatives. It may also be useful to compute key elements of the Hessian numerically, particularly those corresponding to coordinates changing rapidly in the optimization [80]. These approaches are discussed in more detail in Section 10.3.5.

For cases where the current structure is far from the minimum (where the magnitude of the gradient is large) or the PES is very flat (where the Hessian has one or more small eigenvalues), a Newton step may be very large and lead to a point where the model quadratic surface is no longer valid. Circumventing this problem is accomplished by limiting the size of each Newton step [68–71]. There are two closely related methods often used for this purpose: the trust radius method (TRM) and rational function optimization (RFO) [79,81–85].

TRM specifies a maximum step size, know as the trust radius, τ, and limits the size of each step in the optimization to this magnitude. Minimizing the energy in Eq. (13) subject to this constraint, $|\Delta\mathbf{x}| \leq \tau$, gives

$$\Delta\mathbf{x} = -(\mathbf{H} - \lambda\mathbf{I})^{-1}\mathbf{g} \tag{22}$$

where **I** denotes the identity matrix. λ is less than the lowest eigenvalue of the Hessian, less than zero, and is adjusted in order to satisfy the constraint. This ensures that the step

moves downhill on the PES. The TRM step and τ can also be written as

$$\Delta \mathbf{x} = -\sum_{i \geq 1} \frac{\mathbf{v}_i(\mathbf{v}_i^t \mathbf{g})}{b_i - \lambda} \tag{23}$$

$$\tau^2 = \sum_{i \geq 1} \frac{(\mathbf{v}_i^t \mathbf{g})^2}{(b_i - \lambda)^2} \tag{24}$$

where b_i and $\mathbf{v}_i$ are the Hessian eigenvalues and the corresponding eigenvectors. The value of the trust radius can be changed through the course of the optimization depending on how well the estimated energy difference (using Eq. (13)) after each step compares to the actual energy difference. When this difference is small, the trust radius is increased; when it is large, the trust radius is decreased.

RFO can also be used to control the size of the trust radius by minimizing the energy on a rational polynomial approximation to the PES

$$E = E_0 + \frac{\mathbf{g}_0^t \Delta \mathbf{x} + \frac{1}{2} \Delta \mathbf{x}^t \mathbf{H}_0 \Delta \mathbf{x}}{1 + \alpha \Delta \mathbf{x}^t \Delta \mathbf{x}} \tag{25}$$

The parameter α is adjusted to ensure that the step direction leads to a lower energy and that the trust radius is satisfied. This yields equations similar in form to Eqs. (22), (23), and (24). A principle advantage of TRM and RFO is that they step downhill even when the Hessian has one or more negative eigenvalues. Under the same conditions, a raw Newton step will move toward a saddle point. Nevertheless, the character of the structure resulting from a minimization using any algorithm should always be confirmed by calculating the second derivatives and checking that the Hessian has all positive eigenvalues (i.e. all real frequencies).

To ensure that the step lowers the energy and the magnitude of the gradient by a sufficient amount (e.g. the Wolfe condition), it is also important to include an approximate line search [70]. Often, satisfactory results can be achieved by fitting a cubic or constrained quartic polynomial to the energy and gradient at the beginning and end of the step [86]. If the minimum of the line search is within this interval, the energy and gradient can be obtained by interpolation and used in the next Newton step.

For large systems with several hundred atoms, the standard QN algorithms for determining the next geometry step can become a bottleneck. The QN step can also be a bottleneck when the energy evaluation is inexpensive, as is the case when low levels of theory such as molecular mechanics or semi-empirical MO methods are used. Storing the Hessian requires $\mathcal{O}(N^2)$ memory and solving the equations involves $\mathcal{O}(N^3)$ work. One alternative is to use conjugate gradient methods for minimization [70]. The storage and cpu requirements for these methods scale linearly with the system size, but their rate of convergence is significantly poorer than QN methods. Better convergence can be achieved with limited memory QN methods such as L-BFGS [87,88]. In this approach, the Hessian or its inverse is not stored or computed explicitly, but are constructed implicitly as needed. An initial diagonal Hessian, $\Delta \mathbf{x}$, and $\mathbf{g}$ from a fixed number of

the most recent steps are stored. Thus, storage scales linearly with system size. The update of the inverse Hessian is formed implicitly and multiplied by the gradient to get the next step

$$\Delta \mathbf{x} = -\mathbf{H}^{-1}\mathbf{g}, \qquad \mathbf{H}_{k+1}^{-1} = \frac{(\mathbf{I} - \Delta\mathbf{x}_k \Delta\mathbf{g}_k^{\mathrm{t}})}{\Delta\mathbf{x}_k^{\mathrm{t}} \Delta\mathbf{g}_k} \mathbf{H}_k^{-1} \frac{(\mathbf{I} - \Delta\mathbf{g}_k \Delta\mathbf{x}_k^{\mathrm{t}})}{\Delta\mathbf{x}_k^{\mathrm{t}} \Delta\mathbf{g}_k} + \frac{\Delta\mathbf{x}_k \Delta\mathbf{x}_k^{\mathrm{t}}}{\Delta\mathbf{x}_k^{\mathrm{t}} \Delta\mathbf{g}_k}. \quad (26)$$

The computational work involves mostly dot products. If the maximum number of updates is fixed, the work scales linearly. The L-BFGS method has been used in a number of optimization problems in computational chemistry [62,64,89,90].

10.3.2 GDIIS

An alternative optimization method to NR and QN is geometry optimization by direct inversion of the iterative subspace, or GDIIS [91–94]. GDIIS is based on a linear interpolation/extrapolation approach and is very well suited for flat PESs (i.e. one or more eigenvalues of the Hessian are small), where NR can be less efficient. For other situations, the efficiency of GDIIS is roughly the same as NR when the initial structure is near the minimum. However, as discussed below, GDIIS can experience difficulties and a number of modifications to the initial GDIIS approach have been developed to overcome these impediments.

Using a linear combination of the structures from the previous n steps, $\mathbf{q}_1, \ldots, \mathbf{q}_n$, the guess for the next GDIIS structure is

$$\mathbf{q}^* = \sum_{i=1}^{n} c_i \mathbf{q}_i \quad (27)$$

where the coefficients c_i are defined by minimizing the estimated error in $\mathbf{q}^*$. This estimated error, or residuum vector, $\mathbf{r}$, is given by

$$\mathbf{r} = \sum_{i=1}^{n} c_i \mathbf{e}_i \quad (28)$$

where $\mathbf{e}_i$ is an error vector associated with $\mathbf{q}_i$. In practice the minimization of Eq. (28) is done with respect to $|\mathbf{r}|^2$, since $\mathbf{r}$ is a vector. This leads to a least-squares problem to solve for the coefficients, c_i. To estimate the error, two common definitions are used. The first is a NR step,

$$\mathbf{e}_i = -\mathbf{H}^{-1}\mathbf{g}_i \quad (29)$$

and the second is the gradient,

$$\mathbf{e}_i = \mathbf{g}_i \quad (30)$$

Clearly, if the point $\mathbf{q}_i$ is very good (e.g. very near the true PES minimum) then its gradient will be small as will the NR step from this point. Conversely, if $\mathbf{q}_i$ is far from the true PES minimum then $\mathbf{e}_i$ will be large regardless of whether Eq. (29) or (30) is

used. Since an estimate of the error in $\mathbf{q}^*$ is available, the actual GDIIS step makes use of $\mathbf{r}$ in defining the next structure, $\mathbf{q}_{i+1}$.

$$\mathbf{q}_{i+1} = \sum_{i=1}^{n} c_i(\mathbf{q}_i - \mathbf{H}^{-1}\mathbf{g}_i) \tag{31}$$

The NR definition for $\mathbf{e}$, given in Eq. (29), has been used in Eq. (31). If optimization convergence is not met at the point $\mathbf{q}_{i+1}$, then it is added to the collection of structures and a new GDIIS step is taken.

As mentioned above, the efficiency of GDIIS is similar to, and at times greater than, NR. However, GDIIS comes with its share of problems. First, GDIIS tends to converge to the nearest stationary point on the PES, which may or may not be a minimum. For this reason, it is crucial to test the curvature (by computing the Hessian or harmonic frequencies) of an optimized structure that has been found using GDIIS. A second shortcoming of GDIIS is that it can fall into continuous oscillations if it steps near an inflection point (points where one or more Hessian eigenvalues are zero and the magnitude of the gradient is a minimum, but not zero) and the magnitude of the gradient is larger than the convergence criteria of the optimizer. An additional problem develops when many steps are taken. If a large number of points are used in the linear combinations shown in Eqs. (27) and (28) linear dependencies can appear and result in numerical instabilities in the least-squares solution for the expansion coefficients, c_i.

To overcome these deficiencies, Farkas and Schlegel [95] have developed a controlled GDIIS algorithm. Controlling numerical instabilities arising from linear dependencies in Eqs. (27) and (28) can be achieved by limiting the number of points used. Before taking the next GDIIS step, the linear combinations are built one term at a time beginning at the latest point and working back toward the first point. Before adding the next term, near linear dependency is tested for. If the addition of a point indicates a potential numerical instability, only the points used in the GDIIS expansion before the instability are employed.

Farkas and Schlegel [95] also suggested modifications to increase GDIIS's likelihood to converge on a minimum (or TS if desired; see below for further discussion), rather than a higher order saddle point, and to avoid oscillation problems near inflection points. The first modification employs a reference step, such as NR or any other standard minimization method. By comparing each GDIIS step to this reference, steps that head away from the stationary point of interest can be easily detected, and incorporation of RFO or TRM into the NR step (for computing $\mathbf{e}$) can be used to control the GDIIS step direction. Further stability in this regard can be attained by combining the GDIIS and NR (or other standard optimization method) steps. In this way, the actual step taken during the GDIIS optimization results from a weighted mixing of the standard optimization and GDIIS steps. A final modification involves Hessian updating. In general, the convergence of GDIIS is not dependent on the quality of the Hessian. For this reason, early implementations of GDIIS used a fixed Hessian for every step. However, it has been shown that updating the Hessian yields increased stability and efficiency for GDIIS. By implementing the modifications listed above, GDIIS minimization is an attractive optimization algorithm, especially for large systems and for flat PESs.

The GDIIS method and its modifications scale as $\mathcal{O}(N^3)$ with system size because of the need to invert the Hessian and to compute the reference step. If a diagonal Hessian is used and a fixed maximum number of structures are retained in the GDIIS equations, the method becomes linear in work and storage [95,96]. However, the convergence is somewhat slower than the full matrix GDIIS approach. A linear scaling GDIIS method with improved performance can be obtained by combining GDIIS with the L-BFGS approach [87,88] for updating and utilizing the inverse Hessian (see Eq. (26)).

10.3.3 QM/MM optimizations

In recent years much progress has been made to adapt electronic structure calculations to large systems, such as biochemical compounds. One of the more popular advances in this area is the QM/MM approach (QM—quantum mechanics; MM—molecular mechanics) [97–107]. Although there exists a wide variety of QM/MM methods, the basic principle behind them is the same. Namely, a large molecule or system is broken-up into two sections: one that will be treated at a high level of theory—the QM piece—and one that will be treated at a low level of theory—the MM piece. Typically the QM region of the system is defined as the sector where 'the chemistry' is occurring, and the rest of the system is then defined as the MM region. For instance, a QM/MM calculation on an enzyme generally places the active site in the QM region and the rest of the enzyme in the MM region. The ONIOM scheme is a particular type of QM/MM approach that has gained considerable attention because it is a generalized method that can break a system into many layers, which may consist of multiple QM levels, not just one QM region and one MM region [99,108–110].

Because the QM/MM energy, gradient, and Hessian are well defined, one can navigate the combined QM/MM PES. Optimization of the entire system on the QM/MM PES can require many optimization steps and be very costly. Most popular implementations of QM/MM optimization decrease the cost of minimization by employing microiteration schemes [111–114]. The idea here is to alternate between minimization of the QM and MM regions of the system. Since calculations in the MM region are cheap (in terms of computational cost), the typical use of microiterations fully optimizes the MM region after each QM step. Because the QM and MM regions are treated individually and are uncoupled during the optimizations, progress toward the QM/MM PES minimum can be problematic. As a result, traditional microiteration approaches can converge quite slowly or fail, especially when geometric constraints are imposed on the MM region.

One source of this problem is the choice and handling of the coordinate systems of each region during their independent optimizations. Since the MM energy and derivatives are very cheap, it may not be cost effective (in terms of computational time) to use internal coordinates due to the conversion to and from Cartesians (see Eqs. (10), (11), and (12)). However, within the QM region it is still useful to carry out the optimization in internal coordinates. To overcome the difficulties associated with QM/MM optimization using microiterations, Vreven et al. [112] chose a set of coordinates consisting of Cartesian coordinates for the MM region and a set of internal coordinates for the QM region. Furthermore, the Cartesian coordinates in the MM region are

augmented to allow the QM region to undergo overall translation and rotation, which is imperative for cases where constraints in the MM region are present. They also found that this feature slightly improves efficiency when there are no constraints in the MM region. Lastly, their method takes special care to ensure the QM region remains in the same local minimum on the QM PES throughout the MM optimizations.

10.3.4 Finding surface intersections and points of closest approach

The search for conical intersections, avoided crossings and seams of intersection between two PESs are also tasks involving optimization [115–123]. If the two surfaces represent different spin states or have different spatial symmetry, they can cross. If they are the same symmetry and spin, they can interact and the crossing is avoided. Where the matrix element coupling the two surfaces is zero, they touch and give rise to a conical intersection, as illustrated in Fig. 10.3. To study the mechanisms of photochemical reactions, we often wish to find the lowest energy point on a seam or conical intersection. For a seam of intersection between two adiabatic surfaces E_1 and E_2, we require $E_1 = E_2$. Since a (non-linear) molecule has $3N_{\text{atoms}} - 6$ internal degrees of freedom, a seam of intersection has $3N_{\text{atoms}} - 7$ degrees of freedom because of the additional constraint. For a conical intersection, we also require the coupling matrix element, $\mathbf{H}_{12}$, to be zero. Hence conical intersections have $3N_{\text{atoms}} - 8$ degrees of freedom. For molecules larger than triatomic, finding the lowest point on a seam or conical intersection can be quite challenging because of the number of degrees of freedom in the constrained minimization.

One approach to finding the lowest point on a seam or conical intersection is to use Lagrangian multipliers [118–122]. The Lagrangian,

$$L = E_2 + \lambda_1(E_2 - E_1) + \lambda_2 \mathbf{H}_{12} \tag{32}$$

is minimized with respect to λ_1, λ_2, and the geometric coordinates of the molecule so that the constraints $E_1 = E_2$ and $\mathbf{H}_{12} = 0$ are satisfied.

Alternatively, the constraints can be treated using projection methods [123]. Instead of minimizing the absolute value of the energy difference, $|E_2 - E_1|$, it is advantageous to use the square of the energy difference, $(E_2 - E_1)^2$, since this quantity is better suited for quasi-Newton optimization methods. For the remaining $3N_{\text{atoms}} - 7$ or $3N_{\text{atoms}} - 8$ degrees of freedom, the energy of the upper adiabatic surface is minimized. The gradient is given by

$$\mathbf{g} = \frac{\mathrm{d}(E_2 - E_1)^2}{\mathrm{d}\mathbf{x}} + \left(\mathbf{I} - \frac{\mathbf{v}_1\mathbf{v}_1^{\mathrm{t}}}{|\mathbf{v}_1|^2}\right)\left(\mathbf{I} - \frac{\mathbf{v}_2\mathbf{v}_2^{\mathrm{t}}}{|\mathbf{v}_2|^2}\right)\frac{\mathrm{d}E_2}{\mathrm{d}\mathbf{x}} \tag{33}$$

where

$$\mathbf{v}_1 = \frac{\mathrm{d}(E_2 - E_1)}{\mathrm{d}\mathbf{x}} \tag{34}$$

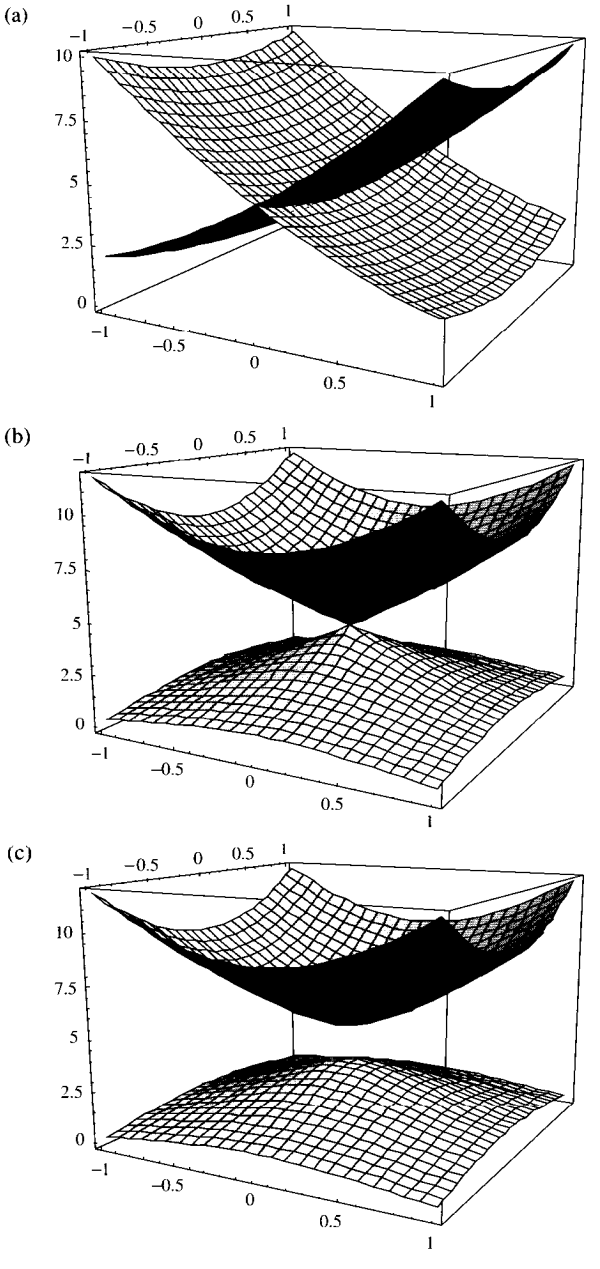

Fig. 10.3. Interactions between two model potential energy surfaces showing (a) a seam, (b) a conical intersection, and (c) a weakly avoided conical intersection (from Ref. [72] with permission).

and

$$\mathbf{v}_2 = \frac{\mathrm{d}\mathbf{H}_{12}}{\mathrm{d}\mathbf{x}} \tag{35}$$

The gradient given by Eq. (33) can be used directly in a conventional unconstrained quasi-Newton optimization algorithm to find the lowest points on seams, avoided crossings, and conical intersections.

10.3.5 Practical considerations

The principle factors affecting the success and efficiency of a minimization calculation are the starting structure provided by the user, the coordinate system, the algorithm to choose the direction and size of the step, the initial Hessian, and the quality of the updated Hessian at later steps. In this section, we discuss these, and other, practical aspects of minimization and offer suggestions for overcoming typical pitfalls. Illustrative calculations have been carried out with the Gaussian series of programs [124] to demonstrate some of these aspects, but the general considerations should also be relevant to other electronic structure codes. Although previous sections have included minimization techniques used with QM/MM calculations and algorithms for locating conical intersections and points of closest approach, the discussion here is focused primarily on standard minimization of structures using electronic structure methods.

10.3.5.1 Starting structure

Obviously the quality of the initial structure provided by the user will affect the success and efficiency of an optimization calculation. The closer the starting structure is to the PES minimum, the faster (in terms of the number of steps taken) the minimization will complete. On the other hand, a poor starting structure can lead to a lengthy calculation and even failure to converge. Preparing a starting structure for minimization is most readily accomplished with the aid of molecular modeling and visualization software. It is also common practice to use experimentally obtained structures (i.e. from crystal structures) when available. Additionally, starting structures can be generated by minimization at lower levels of theory.

While it is clear that a number of viable methods exist for building an initial structure for minimization, it is important to note that optimization calculations cannot yet be treated as black box operations. Instead, a basic understanding of the chemistry of the problem being studied is necessary to ensure that the user is able to properly diagnose problems and determine the appropriateness of an initial structure. For example, consider cyclohexane. From undergraduate organic chemistry classes we know that there are two conformations—chair and boat. Both conformations will have local minima on the PES and using a boat-like structure for the start of a minimization will result in a converged optimization at the boat conformation. If the goal of the optimization is to study the more stable chair conformation this result is not what we want. To get the chair structure, one must start with a chair-like structure. To further illustrate this point, Fig. 10.4 shows a one-dimensional slice of the PES of 1-chloro 2-fluoroethane along the Cl–C–C–F

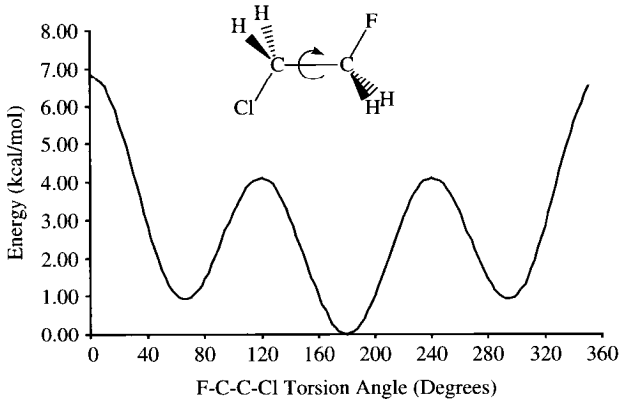

Fig. 10.4. A one-dimensional slice of the potential energy surface of 1-chloro 2-fluorethane along the Cl–C–C–F dihedral coordinate.

torsion angle. In this case there are three local minima on the PES, although the minima at 70 and 290° are mirror images. Again, the initial structure will determine which local minimum the optimizer converges to. Starting an optimization with a Cl–C–C–F dihedral of 30° will lead to the minimum at 70°, while starting at 160° will converge at the global minimum at 180°. One must employ chemical insight when generating the initial structure for minimization. For very complex systems, it may be necessary to generate multiple structures representing different potential conformations, which allows for the study of relative conformational energies, etc.

10.3.5.2 Coordinate system

Another aspect of geometry optimization affecting the success and efficiency of the calculation is the choice of coordinate system. Section 10.2.3 included definitions for different coordinate systems commonly used to describe PESs. Early work in geometry optimization was nearly always done in non-redundant internal coordinates. This coordinate system is easy to use when building acyclic structures and inherently removes rotational and translational degrees of freedom from the system, making it advantageous from an algorithmic standpoint. However, geometry optimization using non-redundant internal coordinates does require some thought since the efficiency, and sometimes the success or failure, of the optimization can depend on the choice of Z-matrix components. An overview of techniques for building effective Z-matrix inputs appeared in an earlier review, and interested readers are referred to that work for a more in depth discussion [80]. Non-redundant internals perform especially poorly in the optimization of polycyclic systems [48–53,63,125]. In these cases, it is better to use Cartesian coordinates than to employ a Z-matrix representation. It has also been shown that mixing non-redundant and Cartesian coordinates can also be useful at times [125].

The most efficient coordinate system, in general, for geometry optimization using electronic structure methods is redundant internal coordinates, especially for cyclic compounds [48–53,63,125]. Table 10.1 shows the number of steps necessary to minimize a set of nine structures using these four different systems. All of the optimizations were

Table 10.1 Comparison of the number of steps required to minimize geometries using various coordinate systems[a]

Molecule	Cartesian	Z-Matrix	Mixed	Redundant internals
2-Fluoro furan	7	7	7	6
Norbornane	5	7	5	5
Bicyclo[2.2.2]octane	19	11	14	7
Bicyclo[3.2.1]octane	6	6	7	5
Endo hydroxyl bicyclopentane	18	8	9	12
Exo hydroxyl bicyclopentane	20	10	11	11
ACTHCP	>80	65	72	27
1,4,5-Trihydroxy anthroquinone	11	10	17	8
Histamine H^+	>100	42	47	19

[a]For complete details see Ref. [51].

started from the same initial geometries [51]. It is clear from this data that for rigid compounds all four coordinate systems are essentially the same. As the flexibility of the molecules increases, the advantage of using redundant internal coordinates becomes increasingly apparent. Because of their obvious benefit, redundant internal coordinates are favored for nearly all geometry optimization calculations used with electronic structure methods.

There are two general problems that can arise in the course of an optimization calculation due to the use of redundant internal coordinates. The first problem is caused by a poorly chosen set of coordinates for the starting structure. Although most programs use an automated mechanism to determine the initial definitions for the redundant internal coordinates, these algorithms are not error proof. To the best of our knowledge, all of the available codes use tables of covalent radii or standard bond lengths, or their equivalent, to determine which atoms are bonded to each other. The user can also define additional internal coordinates. Once the connectivity of the molecule is established, angles and dihedrals can be readily defined. If fragments are detected (i.e. two or more parts of the system that are not connected by bonds), then one, or more, coordinates are added so that the fragments can interact and intermolecular distances can be accounted for. Nevertheless, the tables used to define the initial bonding can ignore important bonds, which can lead to considerably slower convergence. For this reason, it is essential to check the definitions of the redundant internals, which are usually printed out in an output file at the start of the optimization calculation. Our experience has shown that modifications to the redundant internal coordinate definitions are often necessary for transition and inner transition metal complexes.

Another problem that can occur during the course of a minimization in redundant internal coordinates is the internal forces being reported as infinity or undefined [126]. As discussed in Section 10.2.3, the energy derivatives are typically computed in Cartesian coordinates and later converted to internals using Eq. (10). If the redundant internal coordinate definitions become ill defined and/or include linear dependences, then the conversion of forces and Hessians to internal coordinates can become problematic. The easy fix to this problem begins by inspecting the latest structure in the optimization using visualization software to ensure that the structure is reasonable. If all is well, start

the minimization again giving the last structure from the previous optimization as the initial structure for the current calculation. This allows for generation of new coordinate definitions. Again, these definitions should be checked to make sure that all of the critical definitions have been included. In extreme cases, it may be necessary to reduce the redundancy of the coordinate system.

10.3.5.3 Minimization algorithm

The third factor affecting the efficiency of an optimization calculation is the choice of the minimization algorithm. In the sections above we discussed the most common procedures used in practice—QN with RFO or TRM modifications, GDIIS, and controlled GDIIS. The relative efficiencies of these three approaches have appeared in the literature [95], and the results of that work are summarized in Table 10.2. As discussed in Section 10.3.2, regular GDIIS can fall into continuous oscillations near inflection points on the PES. This pathology is experienced in the optimization of five of the eight entries in Table 10.2. The controlled GDIIS method corrects these problems and converges to the appropriate minima. For the first three entries in Table 10.2, regular GDIIS optimization converges to saddle points instead of minima. Again, this problem is solved by using the controlled GDIIS algorithm. Minimization of the smaller systems is equally efficient using controlled GDIIS or QN (with step size and direction control). When larger and more flexible systems are studied, the controlled GDIIS method is often more efficient than QN. Controlled GDIIS is also the recommended method for optimizations on flat PESs and those employing tight convergence criteria.

10.3.5.4 Hessian quality

The final factors affecting optimization are the choice for the initial Hessian and the method used to form Hessians at later steps. As discussed in Section 10.3.1, QN methods avoid the costly computation of analytic Hessians by using Hessian updating. In that section, we also showed the mathematical form of some common updating schemes and pointed out that the BFGS update is considered the most appropriate choice for minimizations. What may not have been obvious from Section 10.3.1 is that the initial

Table 10.2 Comparison of the number of steps required to minimize geometries using QN with RFO, regular GDIIS, and modified GDIIS[a]

Molecule	QN with RFO	Regular GDIIS	Controlled GDIIS
Pterine	36	12[b]	36
Histamine H^+	24	85[b]	25
Hydrazobenzene	25	41[b]	25
ACTHCP	31	–[c]	32
Taxol	64	–[c]	67
For-$(Ala)_{10}$-NH_2	67	–[c]	59
For-$(Ala)_{20}$-NH_2	103	–[c]	93
Crambin	190	–[c]	150

[a]For complete details see Ref. [95].
[b]Attempted minimization yielded a transition state (i.e. first-order saddle point).
[c]Attempted minimization resulted in oscillations about an inflection point.

Hessian does not need to be very accurate. During the optimization the Hessian will be updated, and while the structure moves closer to the PES minimum the Hessian slowly approaches the correct second derivative matrix. In general, the closer the initial Hessian is to the correct Hessian, the faster the optimization will come to convergence.

Most QN optimizations use a Hessian generated from a valence force field or other empirical method. Alternatively, analytic second derivatives can be computed and used for the initial Hessian. This will often decrease the number of steps required to converge to the minimum. However, depending on the size of the system being studied the cost of the initial analytic Hessian calculation may yield a longer overall calculation time than an optimization starting with an estimated Hessian, even though this calculation might require a few more steps. For cases where the starting structure is far from the minimum or when the topology of the PES is not well approximated by a quadratic function (i.e. the Taylor series given in Eq. (13)), Hessian updating may be poor and convergence may be difficult. In these situations it may be necessary to calculate analytic Hessians at every step. In principle this should lead to fewer steps in the optimization, but the additional cost of analytic Hessians will severely increase the overall computational cost for moderate and large systems.

The data presented in Tables 10.3 and 10.4 illustrate some of these issues. Using a set of six compounds, ranging in size from 6 to 72 degrees of freedom, we have carried out optimizations using the identity matrix, an estimated empirical Hessian, and an analytic Hessian for the initial second derivative matrix. Additionally, we have included data for optimizations using analytic Hessians at every step, rather than updating the second derivatives. Table 10.3 shows the number of optimization steps required to complete an optimization using these different approaches to define the initial Hessian, and Table 10.4 contains the relative timing of each calculation. Clearly, using the identity matrix to estimate the initial Hessian is not efficient. For roughly the same cost per step, one can use an estimated Hessian based on empirical force fields [86,127] and achieve a significant improvement in the rate of convergence. However, in the case of pterine and caffeine the identity matrix incorrectly leads the minimization to a saddle point. Since the QN-RFO/TRM method for optimization shifts negative eigenvalues of the Hessian to positive

Table 10.3 Comparison of the number of steps required to minimize geometries (QN with RFO algorithm) using a unit matrix, empirically derived Hessian, and analytic Hessian for the initial Hessian followed by Hessian updating and using all analytic Hessians[a,b]

Molecule	Initial unit matrix with updating	Initial empirical Hessian with updating	Initial analytic Hessian with updating	All analytic Hessians
Ammonia	14	8	6	4
Pterine	22[c]	56	15	10
Caffeine	26[c]	13[c]	67	13
ACTHCP	>100	34	35	15
Histamine H^+	>100	23	30	11
Hydrazobenzene	90	30	29	19

[a]Starting structures taken from Ref. [51].

[b]All calculations carried out at the HF/STO-3G level of theory.

[c]Attempted minimization yielded a transition state (i.e. first-order saddle point).

Table 10.4 Relative timings to minimize calculations using a unit matrix, empirically derived Hessian, and analytic Hessian for the initial Hessian followed by Hessian updating and using all analytic Hessians[a]

Molecule	Initial unit matrix with updating	Initial empirical Hessian with updating	Initial analytic Hessian with updating	All analytic Hessians
Ammonia	2.2	1.3	1.1	1.0
Pterine	5.3[b]	13.8	4.3	8.8
Caffeine	8.5[b]	4.1[b]	12.1	23.0
ACTHCP	>34.5	8.0	8.5	10.7
Histamine H^+	>34.5	4.8	6.4	5.7
Hydrazobenzene	29.8	10.2	11.0	34.3

[a]Convergence data is given in Table 10.3.
[b]Attempted minimization yielded a transition state (i.e. first-order saddle point).

values, describing the curvature correctly for these structures allows the optimizer to properly converge to PES minima when analytic Hessians are used for the initial Hessian. Nevertheless, for most of the compounds studied, and for many structures in general, using an analytic Hessian at the start of the optimization provides very little, if any, improvement to an optimization carried out with an empirically derived Hessian. Moreover, calculating analytic Hessians only at the start of the minimization or at every step can severely increase the computational cost (see Table 10.4).

In general, it is advisable to use an empirical Hessian at the start of a minimization and to update the Hessian using any of the standard methods (see Section 10.3.1). After an optimization has completed, the nature of the stationary point must be confirmed by a calculation of the Hessian. This is not a significant extra burden, since the Hessian at the optimized geometry is also needed to calculate the zero point energy and thermal corrections to the enthalpy. If the Hessian calculation reveals that the optimization has converged to a saddle point (first order or higher), then using an analytic Hessian at the start of the minimization and Hessian updating at subsequent may be best. If this second optimization has also converged to a saddle point, then employing analytic Hessians at every step, or every few steps, may be necessary. What is clear from Table 10.4 is that the decrease in optimization steps using all analytic Hessians does not make up for the cost increase that such a calculation yields. Therefore, using all analytic Hessians in an optimization is best treated as a last resort approach.

10.3.5.5 Tips for difficult minimizations

In this, the last portion of Section 10.3.5, we provide suggestions for solving difficult minimization problems that have not yet been addressed. Specifically, this subsection focuses on problems generally resulting because of the topology of the PES and not because of numerical difficulties arising from the application of a particular method or algorithm.

In the previous section we suggested that analytic Hessians can be used to help converge to a minimum when minimizations using empirical and/or updated Hessians yield first- or higher-order saddle points. Often times, a more cost effective means to achieve the same goal is to slightly distort the offending coordinate and start another minimization using an empirical Hessian at the start with updating thereafter.

As an example, consider a minimization of 1-chloro 2-fluorethane starting with a Cl–C–C–F torsion angle of 125° that has converged to the saddle point at 120° in Fig. 10.4, even though our intent was to find the structure corresponding to the minimum at 180°. We now have a couple of options. One option is to start the calculation over from our initial starting geometry using an analytic Hessian for the initial second derivative matrix. We could also choose to use analytic Hessians at every step or every few steps in the optimization. Alternatively, we could use a molecular graphics package to inspect the imaginary frequency corresponding to the negative Hessian eigenvalue and distort the structure along that normal mode. In this particular case, visualization of this frequency will show motion along the Cl–C–C–F torsion angle distorting the molecule from an eclipsed geometry to a staggered one. Distorting the molecule by setting the Cl–C–C–F angle to roughly 150° will be enough to use an empirical Hessian with updating to converge to the intended minimum. This last option will be much more cost effective since it avoids analytic calculation of the Hessian during the optimization. Of course, a Hessian calculation will still be needed when the calculation has completed to ensure that the newly optimized structure is a minimum on the PES and to obtain the zero point energy.

Another method for removing imaginary frequencies is to utilize constrained optimizations. As the name implies, user defined coordinates are frozen and the remaining coordinates are allowed to minimize. If one or more coordinates have negative Hessian eigenvalues associated with them, it can be useful to freeze all of the other coordinates and allow the offending coordinates to relax. Once the constrained optimization has completed, a frequency calculation is in order to ensure that the imaginary frequency has been removed. If the imaginary frequency still exists, then the other suggestions given above may be helpful and applied together with constrained optimization. After the negative second derivative eigenvalues have been removed, a full optimization (i.e. without any constraints) should follow with a subsequent frequency calculation at the end.

In some very troublesome cases, where only one imaginary frequency remains, a method that can be used as an approach of last resort is to carry out a reaction path following calculation (details on reaction path following are given below in Section 10.5) for a few steps. Starting from a first-order saddle point, a reaction path following calculation will move downhill toward two minima, one of which should correspond to the structure of interest. It is not usually necessary to carry the calculation all the way to the endpoints. After the calculation has been completed the two final structures can be visualized and the appropriate one chosen. If enough steps have been taken this structure should now be near the quadratic region of the minimum and a QN minimization should be able to converge on the intended minimum. However, it may be necessary to calculate analytic second derivatives for the initial Hessian of this optimization.

10.4 TRANSITION STATE OPTIMIZATION

As discussed earlier, minima on the PES correspond to equilibrium geometries and chemical reactions can be described in terms of motion on the PES from one minimum

corresponding to the reactant to a different minimum corresponding to the product. Along the way, the system may pass through other minima, which correspond to intermediates. The motion from one minimum to another can be approximated by the path of least resistance, or the minimum energy pathway (MEP). While moving along the MEP, the system will reach a point of highest energy—the transition state (TS). Turning back to the mountain range analogy from Section 10.2, the TS is at the top of the lowest mountain pass connecting two valleys. The TS will have one (and only one) direction of downward curvature, which points in the direction of the reactant minimum on one side and the product minimum on the other. In all other directions, the TS will have local upward curvature. A stationary point (a point where the first derivatives are zero) with this topology is known as a first-order saddle point. A *n*th-order saddle point has *n* directions of downward curvature. In terms of the Hessian, this means that the TS will have one (and only one) negative Hessian eigenvalue and all of the other Hessian eigenvalues will be positive. Since the Hessian is the system's force constant matrix and the vibrational frequencies are proportional to the square root of the eigenvalues of the mass-weighted Hessian, the TS will have one (and only one) imaginary frequency. The eigenvector corresponding to the imaginary frequency is known as the transition vector because it corresponds to molecular displacement along the reaction path through the TS.

A number of good reviews on TS optimization have appeared in recent years [9,11, 12,21,23–25,128]. In this section, we provide an overview of the three general classes of TS optimization methods—local schemes (Section 10.4.1), climbing, bracketing, and interpolation algorithms (Section 10.4.2), and path optimization approaches (Section 10.4.3). In Section 10.4.4 we discuss practical considerations related to TS optimization and offer suggestions for difficult cases.

10.4.1 Local methods

Many of the standard minimization algorithms presented in Section 10.3 can be modified to find TSs. Such methods are commonly referred to as local methods. Unfortunately, simple applications of QN methods are often unsuccessful in TS searches. The problem stems from the fact that they will only converge to the TS if the initial guess falls within, or very near, the quadratic region of the true TS, which is generally much smaller than for a minimum. This means the error tolerance in the starting structure is much less for TS optimization than for minimization. Therefore, it is necessary to ensure the Hessian has an appropriate eigenvector with a negative eigenvalue for a QN step to move closer to the desired TS. Despite these difficulties, good chemical intuition (sometimes along with a bit of luck) can provide adequate guesses for TSs to be found using local methods.

The adaptation of most minimization algorithms, such as QN and GDIIS, for TS optimization is rather straightforward [68–71,93–95]. Just as with minimization it is common to use Hessian updating. Unlike minimization, though, the BFGS updating scheme is unacceptable in TS optimization because it forms positive definite Hessians. When the Hessian becomes negative definite, as is the case near the TS, the BFGS formula becomes ill conditioned [129].

The Murtaugh–Sargent update, which was already discussed in Section 10.3.1, is one option [79,130,131]. Another common choice is the Powell-symmetric-Broyden (PSB) update, which was first recommended for TS optimization by Simons et al. [132]. A PSB updated Hessian is given by

$$\Delta\mathbf{H}^{\mathrm{PSB}} = \frac{(\Delta\mathbf{g} - \mathbf{H}^{\mathrm{old}}\Delta\mathbf{x})\Delta\mathbf{x}^{\mathrm{t}} + \Delta\mathbf{x}(\Delta\mathbf{g} - \mathbf{H}^{\mathrm{old}}\Delta\mathbf{x})^{\mathrm{t}}}{\Delta\mathbf{x}^{\mathrm{t}}\Delta\mathbf{x}} - \frac{\Delta\mathbf{x}^{\mathrm{t}}(\Delta\mathbf{g} - \mathbf{H}^{\mathrm{old}}\Delta\mathbf{x})\Delta\mathbf{x}\Delta\mathbf{x}^{\mathrm{t}}}{(\Delta\mathbf{x}^{\mathrm{t}}\Delta\mathbf{x})^2} \tag{36}$$

Bofill [79,89,129–131,133] has developed a hybrid updating scheme with better performance for TS optimization. The Bofill update mixes MS and PSB solutions giving

$$\Delta\mathbf{H}^{\mathrm{Bofill}} = \phi\Delta\mathbf{H}^{\mathrm{MS}} + (1-\phi)\Delta\mathbf{H}^{\mathrm{PSB}} \tag{37}$$

where

$$\phi = \frac{(\Delta\mathbf{x}^{\mathrm{t}}(\Delta\mathbf{g} - \mathbf{H}^{\mathrm{old}}\Delta\mathbf{x}))^2}{\Delta\mathbf{x}^2(\Delta\mathbf{g} - \mathbf{H}^{\mathrm{old}}\Delta\mathbf{x})^2} \tag{38}$$

and $\Delta\mathbf{H}^{\mathrm{MS}}$ is given by Eq. (20).

10.4.2 Climbing, bracketing, and interpolation methods

Since local methods will, in general, only succeed in finding a TS if the initial geometry lies within the quadratic region of the first-order saddle point and the initial Hessian has an appropriate eigenvector with a negative eigenvalue, the fate of TS optimization by local methods rests in one's ability to apply chemical intuition to problems that, at an ever increasing rate, are anything but intuitive. To overcome this difficulty, a number of methods have been developed that automate the initial guess procedure for TS optimization. Using information provided by the user, these algorithms produce an initial guess at the TS by climbing uphill from one minimum, or by bracketing or interpolating a TS between the reactant and product minima. After the region of the TS is located by one of these methods, the structure can be improved using local TS optimization. Again, the literature abounds with climbing and walking, bracketing, and interpolation schemes [26, 84,132,134–152]. Here, we will consider coordinate driving, shallowest ascent and walking up valleys, linear and quadratic synchronous transit, synchronous transit-guided quasi-Newton, and ridge following.

For a limited number of reactions, the reaction pathway can be described by a scan of the PES along one (internal) coordinate. The most prevalent classes of reactions falling into this category are conformation and bond dissociation reactions, where a change in a torsion angle describes the reaction for the former and a bond stretch coordinate describes the latter. Climbing methods making use of this principle are often referred to as 'coordinate driving' algorithms. Beginning at a PES minimum (i.e. the reactant or product), the method traces a path along the coordinate of interest by incrementing its value from reactant to product minima. At each increment, the energy of the new structure is calculated and the highest energy structure on the pathway is taken as an estimate for the TS, which can be used in a local TS optimization calculation. Since other

internal coordinates are affected by changes in the driven coordinate, most applications of this approach include a constrained optimization of the other $N - 1$ coordinates at each increment. This provides a much better guess than a rigid scan. Although coordinate driving can yield a good estimate for the TS, it can be costly if small increments are necessary. Additionally, constrained optimization at each step will increase the computational cost since multiple energy and gradient calculations will be required at each point in the scan. If more than one coordinate are involved in the reaction, coordinate driving will not provide an adequate estimate of the TS. Further difficulties, such as discontinuities, can be encountered if the reaction path is strongly curved [153–155]. The reduced gradient following (RGF) method is an improved version of coordinate driving that is better able to handle curved reaction paths [156–161]. The RGF approach works by defining a path that connects stationary points on the PES according to the differential equation

$$\mathbf{r} - \frac{\mathbf{g}[\mathbf{x}(t)]}{|\mathbf{g}[\mathbf{x}(t)]|} = 0 \tag{39}$$

At each point in the RGF point, the gradient, $\mathbf{g}$, has a constant direction given by the unit vector $\mathbf{r}$. Typically, this direction is chosen in a similar manner to the coordinate driving algorithms. As we will see in Section 10.5, the second term in Eq. (39) comes from the steepest descent path definition used in reaction path following [162].

An alternative to coordinate driving is the 'shallowest ascent', 'eigenvector following' or 'walking up valleys' approach [26,84,132,134–137,143–145]. There are two general flavors of walking up valleys algorithms—one requires the structure of either the reactant or the product, while the other uses the structures of both minima. Starting at one minimum, one can walk uphill along the shallowest ascent direction by following the Hessian eigenvector corresponding to the lowest eigenvalue. The need for the Hessian at each step can make this method costly. As a result, most implementations employ Hessian updating. In order to assure that the shallowest ascent direction is followed, and to minimize along all other directions, methods similar to RFO and TRM have been implemented. In this way, each step is defined according to

$$\Delta\mathbf{x} = -(\mathbf{H} - \lambda\mathbf{I})^{-1}\mathbf{g} \tag{40}$$

The parameter λ is chosen such that $(\mathbf{H} - \lambda\mathbf{I})$ has only one negative eigenvalue and the step has an appropriate length. The use of Eq. (40) is also at the heart of successful local TS optimization methods and greatly expands the radius of convergence for TS optimization. Different values for λ can be used for the directions corresponding to the uphill climb and the downhill minimization [83,85,134]. However, following the shallowest ascent path may not necessarily lead to the correct TS. This issue is addressed by considering the model surface shown in Fig. 10.1. Although the shallowest ascent pathway from Product A correctly leads to the TS connected to the reactant, the shallowest ascent pathway from the reactant does not head toward the same TS. Instead, it leads to Product B.

Another interpolation method using structural information from the reactant and product minima is linear synchronous transit (LST) [139]. These two points on the PES

can be used to form a rough approximation for the reaction pathway by interpolating a line between them. The maximum (in terms of energy) along this line serves as an upper bound to the TS. Although the Hessian at the LST maximum often has more than one negative eigenvalue, it is usually a satisfactory estimate for the TS and can be refined using a local optimization method.

An improvement to LST is incorporated in the quadratic synchronous transit (QST) method [139,148,149]. QST begins with the LST maximum and minimizes perpendicular to the LST path. Then, a new quadratic pathway is interpolated using this new approximate TS, the reactant, and the product. The maximum point on the QST pathway is located and serves as the QST estimate for the TS. For some reactions the LST and QST estimates can be quite similar. However, systems with curved reaction paths can show significant differences between the LST and QST estimates. As before, the estimated TS can be refined by a local method, using Eq. (40) to control the step size and direction. A variation of QST is synchronous transit-guided quasi-Newton (STQN) [138], which directly combines QN with LST or QST. STQN also uses the arc of a circle for the estimated path. The algorithm takes a limited number of initial steps to maximize the energy along the LST or QST path, and then heads toward the TS using the Hessian eigenvector that overlaps best with the LST/QST path. The Hessian eigenvalues are adjusted according to Eq. (40).

Fig. 10.5 shows the LST and QST pathways and their estimated TSs on a model PES. For some reactions, for instance Reactant → Product B, both pathways agree. For other reactions, for instance Reactant → Product A, the LST pathway can differ from the QST path. It is clear that for the latter case the QST estimate for the TS is much closer to the actual TS. For some reactions with strongly curved paths, QST and STQN interpolations can be enhanced by a user-supplied guess at the TS that differs from the automated search result [138].

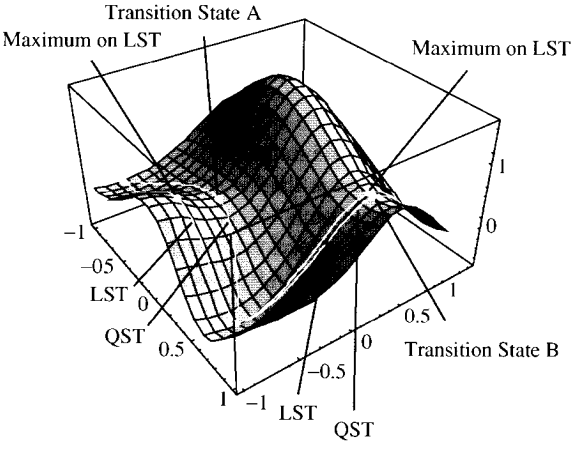

Fig. 10.5. Model potential energy surface illustrating linear synchronous transit (LST) and quadratic synchronous transit (QST) paths (from Ref. [72] with permission).

The ridge following method of Ionova and Carter [146,147] can be viewed as another modified version of LST. This approach begins with reactant and product structures and interpolates a line between them. In the same way as LST, an initial estimate for the TS is determined by finding the highest energy point on the linear path. Instead of feeding this point into a local method, the ridge following algorithm now picks two points on the LST pathway that lie on either side of the estimated TS. The distance between these points is kept small, and they are both allowed to move downhill toward the reaction path. Each step in the progression toward the reaction path and the TS is controlled by side step followed by a downhill step. Let $\mathbf{x}_i^a$ and $\mathbf{x}_i^b$ be the structures of the two points that straddle the TS ridge, where a maximum energy structure $\mathbf{x}_i^*$ exists on the line $(\mathbf{x}_i^a, \mathbf{x}_i^b)$. The side-step portion finds two new points, $\mathbf{x}_i^{a'}$ and $\mathbf{x}_i^{b'}$, which are on the line $(\mathbf{x}_i^a, \mathbf{x}_i^b)$ and are found according to

$$\mathbf{x}_i^{a'} = (\mathbf{x}_i^* + s\mathbf{p}_i), \qquad \mathbf{x}_i^{b'} = (\mathbf{x}_i^* - s\mathbf{p}_i) \tag{41}$$

where

$$\mathbf{p}_i = \frac{\mathbf{x}_i^{b'} - \mathbf{x}_i^{a'}}{|\mathbf{x}_i^{b'} - \mathbf{x}_i^{a'}|} \tag{42}$$

and s is a side-step step size. The downhill step is then given by

$$\mathbf{x}_{i+1}^a = \mathbf{x}_i^{a'} - u\mathbf{g}_i^{a'}, \qquad \mathbf{x}_{i+1}^b = \mathbf{x}_i^{b'} - u\mathbf{g}_i^{b'} \tag{43}$$

where u is the size of the downhill step, $\mathbf{g}_i^a$ and $\mathbf{g}_i^b$ are the gradients at $\mathbf{x}_i^{a'}$ and $\mathbf{x}_i^{b'}$, and $\mathbf{x}_{i+1}^a$ and $\mathbf{x}_{i+1}^b$ give the next set of structures along the ridge. Alternatively, the step can be taken along the gradient at $\mathbf{x}_i^*$. In either case, it can be shown [146] that unless the gradient at $\mathbf{x}_i^*$ is zero, values of s and u can be chosen such that there is a maximum of energy on the line connecting the next set of points, $\mathbf{x}_i^{a'}$ and $\mathbf{x}_i^{b'}$, and that this energy is lower than the maximum on the line connecting the previous set of points. One can think of this process as a constrained optimization following the ridge from a second- (or higher-) order saddle point to the first-order saddle point. When the component of the gradient perpendicular to the line between the two points is zero, or very near zero, they lie close to the reaction path and an intermediate point between them provides a very good estimate for the TS. A local TS optimization method can then be used to converge the ridge following TS to the stationary point.

A novel interpolation method proposed and refined by Jensen and others uses MM or valence bond PESs [140–142,150–152]. Earlier we mentioned that most MM methods do not properly describe reactive systems. This is due to the fact that atom types and molecular connectivity define the force fields generating the MM PES. Therefore, motion on the PES involving bond breaking or bond making is discontinuous. Jensen's approach makes use of this characteristic and treats the MM PESs of the reactant and product as separate surfaces that intersect and form a seam. One can then find the minimum on this seam and use the corresponding molecular configuration as the initial guess for the TS, which is optimized using a local TS optimization method on an electronic structure PES. The problem of finding this point on the intersecting seam is equivalent to the task

of finding points of closest approach and minima on seams between different electronic state PESs (see Section 10.3.4) [115–123].

10.4.3 Path optimization methods

Clearly, the principle obstacle to interpolation methods is the choice of the approximate reaction pathway. A series of methods have been developed to find not just the TS, but the entire MEP. As a class of algorithms, these approaches have been called chain of states and path optimization methods [163]. Starting with the reactant and product structures as input, these methods search for the MEP by minimizing the energy of a number of points, known as images, which lie on an initial interpolated pathway. As a result, many energy and derivative calculations are required for each image making path optimization methods generally much more expensive than interpolation methods. However, path optimization provides a means for finding TSs while simultaneously elucidating the MEP (or at least a good approximation) without *a priori* knowledge of the TS or the curvature of the reaction path, making it an effective and robust alternative to the other approaches discussed above. Path methods are especially useful for difficult problems where the previously described methods fail to converge to a first-order saddle point or the TS of interest.

In this section, we begin by outlining the elastic band theory of Elber and Karplus [164], which forms the basis for most, if not all, of the development of chain-or-states methods. We then outline two popular methods that correct some of the failures of elastic band theory: the nudged elastic band (NEB) method [165] and the path optimization algorithm of Ayala and Schlegel [166]. Lastly, we consider approaches that develop the reaction pathway by growing separate paths from the reactant and product minima, which have been referred to as growing string methods [167]. Using any of these algorithms provides an estimate for the TS that is usually quite good (as opposed to the rough approximation to the TS provided by LST). Nevertheless, full TS optimization using a local approach is still advisable if one wishes to elucidate an accurate barrier height or characterize the TS geometry.

The elastic band method developed by Elber and Karplus [164] is based on the minimization of a line integral, which has the form

$$S(\mathbf{q}_\mathrm{i}, \mathbf{q}_\mathrm{f})_L = \frac{1}{L}\int_{\mathbf{q}_\mathrm{i}}^{\mathbf{q}_\mathrm{f}} [\mathbf{G}(\mathbf{q})\mathrm{d}\mathbf{l}(\mathbf{q})]_L \tag{44}$$

where S is the objective function (the function that will be optimized), $\mathbf{q}_\mathrm{i}$ and $\mathbf{q}_\mathrm{f}$ are the coordinates for the initial and final structures in the reaction (i.e. reactant and product configurations), $\mathbf{G}$ is a vector that is a function of the system coordinates given by

$$\mathbf{G}(\mathbf{q}_j) = E_j \mathbf{u}_j \tag{45}$$

and $\mathrm{d}\mathbf{l}(\mathbf{q})$ is an infinitesimal line segment on the path $\mathbf{L}$ of length L. In Eq. (45) $\mathbf{u}_j$ is a unit vector in the direction $\mathbf{q}_j - \mathbf{q}_{j-1}$. The path $\mathbf{L}$ begins as the initial guess at the reaction path, which we seek to modify and relax to the MEP. In order to find the path $\mathbf{L}$ that

minimizes S, Eq. (44) must be discretized. This results in a series of M points, $\mathbf{q}_1$ through $\mathbf{q}_M$, being placed along $\mathbf{L}$ between the reactant and product structures, $\mathbf{q}_0$ and $\mathbf{q}_{M+1}$. Substituting Eq. (45) into (44) and discretizing yields

$$S(\mathbf{q}_0, \mathbf{q}_{M+1})_L = \frac{1}{L} \sum_{j=1}^{M} E_j \mathbf{u}_j \cdot \Delta \mathbf{l}_j \tag{46}$$

where

$$\Delta \mathbf{l}_j = l_j \mathbf{u}_j \tag{47}$$

Substitution of Eq. (47) into Eq. (46) gives

$$S(\mathbf{q}_0, \mathbf{q}_{M+1})_L = \frac{1}{L} \sum_{j=1}^{M} E_j l_j \tag{48}$$

In the original implementation, Elber and Karplus also found it necessary to add two penalty functions to Eq. (44) that avoid rotation by the images and also keep the images from collecting to one location on the path, i.e. in the minima wells and flat regions of the path [168]. Other pitfalls of the elastic band method include a failure to actually converge to a reaction pathway without a large number of images and for the path to develop kinks and to turn back on itself. Subsequent work by Elber and coworkers [164,168–171] and others [172–175] sought to correct these difficulties and resulted, most notably, in the development of the self-penalty walk [168–171] and locally updated planes algorithms [168,171]. However, most present-day implementations of the basic ideas put forth in elastic band theory are best encapsulated in discussions of the path optimization [166] and NEB approaches [165,176].

In the path optimization method [166] a series of constrained optimizations is used to find the transition state and points on the steepest descent reaction path. The path is relaxed by applying a QN-like optimization scheme on each image in turn, in a manner resembling the reaction path following algorithm developed by Gonzales and Schlegel [177,178] (see Section 10.5.2). Microiterations are used to simultaneously relax the images toward the reaction path and maintain even spacing. The highest energy point on the path is optimized to the TS using a modified version of the STQN optimization algorithm discussed in Section 10.4.2 [138]. Additionally, an initial guess for the TS can be provided by the user to better define the initial path.

The original elastic band approach places 'springs' between successive images to prevent them from falling down into the minima. Adding the springs, with a force constant k, gives the objective function, S, as

$$S(\mathbf{q}_0, \mathbf{q}_{M+1})_L = \sum_{j=1}^{M} E_j + \sum_{j=1}^{M} \frac{k}{2} l_j^2 \tag{49}$$

Many of the problems with elastic band theory are rooted in this definition and their effect on the relaxation of the path. The effective elastic band force acting on image j, $\mathbf{F}_j^{\mathrm{EB}}$, in

this method is a modified force that is dependent upon k,

$$\mathbf{F}_j^{\mathrm{EB}} = \mathbf{F}_j + \mathbf{F}_j^{\mathrm{spring}} \tag{50}$$

where

$$\mathbf{F}_j^{\mathrm{spring}} = (k\mathbf{l}_{j+1} - k\mathbf{l}_j) \tag{51}$$

Recall that $\mathbf{F} = -\mathrm{d}E/\mathrm{d}\mathbf{x}$. The first term in Eq. (50) is the 'true' force and the second term is known as the 'spring' force. If k is too large the elastic band becomes stiff and the final path will not converge to the MEP. Instead, the elastic band path will cut corners. If k is too small, the images begin to slide down the path to the two minima wells.

A simple correction to these problems is achieved by projecting out the parallel (with respect to the path) component of the true force and the perpendicular (with respect to the path) component of the spring force before evaluating Eq. (50). In this way, the images are 'nudged' in the optimal direction, i.e. toward the MEP, while the springs carry out their intended responsibility. Hence, the method is known as NEB [165,179]. Now, the effective force is given by

$$\mathbf{F}_j^{\mathrm{EB}} = (\mathbf{I} - \hat{\tau}_{\parallel}\cdot\hat{\tau}_{\parallel}^{\mathrm{t}})\mathbf{F}_j + (\hat{\tau}_{\parallel}\cdot\hat{\tau}_{\parallel}^{\mathrm{t}})\mathbf{F}_j^{\mathrm{spring}} \tag{52}$$

where $\hat{\tau}_{\parallel}$ and $\hat{\tau}_{\perp}$ are unit vectors pointing parallel and perpendicular to the path. The definitions of $\hat{\tau}_{\parallel}$ and $\hat{\tau}_{\perp}$ can greatly affect the success of an NEB calculation and a number of different definitions have been contemplated and applied [165,179]. Regardless of the choice for the tangent vectors, NEB tends to maintain good spacing along the path. However, NEB is not without its problems. In order to get a smooth path a large number of images are often required, which in turn makes NEB a very costly method. Furthermore, the standard implementation of the method relaxes the path using the velocity Verlet algorithm, a scheme used in classical dynamics. The result is that many path relaxation iterations are often necessary before convergence is satisfied. Modifications to NEB have included dynamic adjustment of the end points to focus on regions of specific interest and choosing one image to climb uphill toward the TS [176, 180]. The L-BFGS algorithm (see Section 10.3.1) can be employed in the image relaxation steps to decrease the cpu and memory cost of NEB [181–183]. Another efficient extension of NEB, known as the replica path scheme, has been developed by Brooks and coworkers [184]. All of these developments dramatically cut down on the total cost of the calculation by leading to faster and more stable path convergence.

Another class of TS optimization algorithms is based on a 'burn the wick from both ends' principle. These methods begin at the reactant and product minima and grow two pathways that communicate and simultaneously head toward the TS. These approaches are possibly best described as hybrids of path optimization and bracketing philosophies. They have been included here in order to draw on the ideas presented above and also because the calculation yields an estimate for the reaction pathway that, in many cases, is a very good approximation to the MEP. In this regard, these methods are very similar to the path optimization schemes just discussed. The most basic application of this idea was originally encompassed by the saddle method [144], which begins by considering the coordinates of the reactant and product structures, $\mathbf{R}$ and $\mathbf{P}$, which are a distance δ apart

on the PES. Let $\mathbf{R}'$ and $\mathbf{P}'$ denote the coordinates of the current step in the reactant and product valleys, respectively. One can simultaneously walk up these two valleys by letting the lower energy structure take a step that decreases δ by a small amount (i.e. 5–10%) followed by a minimization that constrains the distance between $\mathbf{R}'$ and $\mathbf{P}'$. This process is repeated enough times to converge to an estimate for the TS. Similar methods present in the earlier literature include the sphere optimization technique [185] and the locally updated planes method [168].

The most recent addition to this category of TS optimization methods is the growing string approach of Peters et al. [167]. The growing string algorithm is based on a modified version of the string path optimization scheme, which redistributes the images along the interpolated pathway after each minimization step [186]. In the simplest case, the redistribution step uniformly spaces the images along the path. This step can also distribute the images in an uneven manner. For instance, a higher density of images can be used near the TS or regions of the path with large curvature. Additionally, the number of images can be dynamically modified during the calculation. The growing string method makes use of all of these options by growing two strings, one from the reactant well and one from the product well. These individual strings are allowed to relax and the images along each string are redistributed after each step. When the force normal to the path is small at a frontier image (the image on each string closest to the TS), an additional image is added to the local string. After the two frontier images are close to each other, the two strings are merged and the TS optimization can be completed using a local method. This method has been shown to require fewer energy and gradient calculations than traditional path optimization schemes [167], making it an attractive alternative to the path optimization algorithms already discussed.

10.4.4 Practical considerations

In this section, we consider a few points related to the practical application of the methods described above for TS optimization. The factors affecting TS optimization are the same as for minimization: the starting structure provided by the user, coordinate system, algorithm choice, initial Hessian, and quality of the updated Hessian. Since the points made in Section 10.3.5 are also valid for TS optimization, we do not restate them here. Instead, we focus on specific issues unique to TS optimization and recommend that the reader first read Section 10.3.5. This section also contains suggestions for difficult TS problems.

10.4.4.1 Building an initial structure

For local methods, it can be difficult to build a guess at the TS structure. Using a guess at the TS is also useful for interpolating, bracketing, and path optimization methods. However, generating an initial structure of a TS is usually non-trivial. Unlike minima, there are no direct experimental observations of TS geometries. Instead, the best tools available to computational chemists for this purpose are chemical intuition and the theoretical literature. Over the past two decades, thousands of optimized TSs have been

reported in the literature for a vast array of reaction classes. Here, we offer some general suggestions based on these data and our own experience.

Initial TS structures for unimolecular reactions, such as ring closures, hydrogen transfers, internal isomerizations, etc. are most easily built after the reactant and product structures have been minimized. Using these two structures, a TS guess can be made by choosing a molecular configuration lying between the two ground state structures that lines up along a reasonable reaction pathway. The requirement that the structure lie along a reasonable reaction pathway is crucial to the success of the TS optimization. For instance, consider the rearrangement reaction HCN → HNC. Both minima are linear, and choosing a structure that lies exactly between them (i.e. by averaging the Cartesian coordinates) produces a configuration that places the H atom in the middle of the C–N bond. Obviously, this is not a viable TS. A more reasonable reaction path has the H atom moving in a arc starting where the H atom is bonded to C and the H–C–N angle is 180°, passing through a structure where the H atom lies above the C–N bond and the three atoms form a triangle, and finishing with the H atom bonded to N and the C–N–H angle is 180°. A suitable guess for most bimolecular reactions can be generated by setting the lengths of the bonds being formed to 80–120% longer than equilibrium [52].

When the cost of a frequency calculation is reasonable, it can be useful to evaluate the Hessian for the TS guess structure. The purpose of this calculation is twofold: (1) to see if the initial guess has one, and only one, imaginary frequency; and (2) to see if this imaginary frequency corresponds to a reasonable displacement given the reaction being studied. If the guess structure does not have any imaginary frequencies, using a rigid scan along the perceived reaction coordinate and taking the highest energy structure in the scan can often yield an appropriate guess. For cases where multiple imaginary frequencies exist, there are two options. The first option, which is best when the largest magnitude imaginary frequency corresponds to the reaction coordinate and the other imaginary frequencies are much smaller in magnitude (i.e. one or more orders of magnitude difference), is to use this structure and carry out the TS optimization nevertheless. Often, the other imaginary frequencies will relax and the optimization algorithm will find the correct TS. The second option is to freeze the internal coordinate(s) corresponding to the reaction path and minimize the structure for a few steps (~ 10–20). This approach is best when the reaction coordinate has an imaginary frequency that is not the largest in magnitude or the additional imaginary frequencies are the same order of magnitude as the correct imaginary frequency. After a few steps of minimization the Hessian can be reevaluated. If the erroneous imaginary frequencies have become real or the conditions for the first option are met, the current structure can be used for the TS optimization. Otherwise, the process should be repeated.

10.4.4.2 Coordinate system

The coordinate system choice is also important in TS optimization. As with minimization, redundant internal coordinates have been shown to be the best choice for TS optimization [52]. Table 10.5 compares the number of optimization steps required for convergence using the three-structure STQN method with Z-matrix and redundant internal coordinates. Clearly, redundant internals work best. In Section 10.3.5.2, we advised that users check the redundant internal coordinate definitions to ensure all of

Table 10.5 Comparison of the number of steps required to optimize TS geometries using three point STQN with various coordinate systems

Reaction[a]	Z-Matrix internals	Redundant internals
$CH_4 + F \rightarrow CH_3 + HF$	6	5
$CH_3O \rightarrow CH_2OH$	9	9
$SiH_2 + H_2 \rightarrow SiH_4$	11	8
$C_2H_5F \rightarrow C_2H_4 + HF$	15	11
Diels–Alder reaction	23	14
Claisen reaction	15	15
Ene reaction	28	18

[a]For complete details see Ref. [51].

the coordinates are included in the definitions. The same issue arises in TS optimization. It is imperative that the redundant internal definitions include all of the coordinates relevant to the reactant and the product. Methods using these structures in their input can generate the union of the reactant and product internals for the TS coordinate definitions. However, local methods are not able to make use of that additional information and other coordinates will often need to be defined.

10.4.4.3 Algorithm choice

The algorithm chosen to carry out a TS optimization can dramatically affect the success of the optimization and the efficiency of the calculation. Unfortunately, a thorough comparison of all of the methods discussed above is not yet available in the literature and is beyond the scope of this review. Nonetheless, Table 10.6 is included to show a general comparison of the efficiency of local, interpolating, and path optimization methods. Specifically, we have used the QN local TS optimization, three point STQN, and path optimization approaches. The interpolating method has roughly the same cost or less cost than the local method. For the ene reaction, the local method is unable to optimize to the TS while the interpolating algorithm converges to the proper TS within 20 steps. The path optimization method also performs well. However, the path method requires many more energy and derivative evaluations since it must compute this information for each image each time a step is taken.

Table 10.6 Comparison of the number of gradient evaluations required to complete TS optimization using a QN with RFO, three point STQN methods, and the path optimization[a]

Reaction	QN with RFO	Three point STQN	Path optimization
$CH_3O \rightarrow CH_2OH$	12	9	51
$SiH_2 + H_2 \rightarrow SiH_4$	11	8	47
$C_2H_5F \rightarrow C_2H_4 + HF$	16	11	73
Diels–Alder reaction	56	14	41
Ene reaction	Fail	18	101

[a]For complete details see Refs. [138,166].

10.4.4.4 Hessian quality

The quality of the Hessian significantly affects the behavior of TS optimization. Generally speaking, the cost issues raised in Section 10.3.5.4 also hold for locating TSs. One notable difference for TS optimization is that the ability of the algorithm to converge to a first-order saddle point is much more sensitive to the initial Hessian quality. For this reason, using an analytic Hessian at the start of the optimization is very useful, provided that the cost of the Hessian is not too large. Analytic Hessian calculations can be prohibitively expensive for many systems. In these cases, an empirical Hessian can work well provided that it has a suitable negative eigenvalue and eigenvector. Another method often used to generate the Hessian is to use second derivatives computed at a lower, and cheaper, level of theory. For example, a HF/3-21G Hessian can be used at the start of a TS optimization at the HF/6-311G(d) level. An alternative approach is to analytically or numerically calculate the rows and columns of the Hessian that are important in the reaction coordinate [52,80,138]. The other elements can be determined using standard force field estimates [127].

10.4.4.5 Verifying TSs

After a TS optimization has completed, it is always necessary to verify the structure. Verification of a TS consists of two steps. First, the Hessian must be evaluated at the optimized structure and diagonalized to ensure that there is one, and only one, negative eigenvalue. The second step in verifying an optimized TS is to test if the saddle point lies on a path connecting the intended reactant and product minima. This task is readily accomplished by employing reaction path following (see Section 10.5) and/or by visualizing the displacement along the vibrational mode corresponding to the imaginary frequency. For instance, consider the rearrangement reaction of HCN → HNC. Visualization of the TSs imaginary frequency clearly shows movement of the H atom from C to N. Some reactions have curved reaction paths and visualization of the TSs imaginary frequency may not directly indicate that the TS is connected to the reactant and product. In these cases, reaction path following is required. If either verification test fails, the optimized TS is not a valid structure and the search for the proper structure must be restarted.

10.5 REACTION PATH FOLLOWING

After a TS has been located, it is necessary to confirm that it lies on a pathway connecting the requisite reactant and product. This can be done by following the path of steepest descent downhill from the TS to reactant and product PES minima. Following the reaction path can also show if any intermediates lie between the reactant and product. A reaction path determined in isoinertial coordinates (i.e. a coordinate system where all of the coordinates are scaled to have the same reduced mass) is known as a MEP [187–191]. Using the structure and vibrational frequencies at the TS, one can apply TST to determine rates of reaction. Knowing the MEP, especially near the TS, allows one to employ more sophisticated methods for determining reaction rates such as VTST and RPH methods [3–7]. Gradient extremals [137,192–196] also define paths across PESs, but because they do not necessarily connect stationary points as directly as MEPs we do not consider

them further in this context. Also beyond the scope of this review are methods that determine the free energy along an MEP [114,197–205]. Interested readers should consult the literature.

The actual path mapped out by the MEP on the PES is dependent on coordinate system. However, changes in coordinate system do not alter the nature of the stationary points on the PES (i.e. minima, TSs, etc.). One coordinate system, mass-weighted Cartesian coordinates (see Section 10.2.3), is especially significant for reaction dynamics, and the MEP in this coordinate system is known as the intrinsic reaction coordinate (IRC) [162]. In this section, we use the terms MEP, IRC, steepest descent path, and reaction path synonymously.

The starting point for mathematically defining the MEP is a Taylor expansion of the PES.

$$E(\mathbf{x}) = E_0 + \mathbf{g}_0\Delta\mathbf{x} + \frac{1}{2}\Delta\mathbf{x}^t\mathbf{H}_0\Delta\mathbf{x} + \cdots \tag{53}$$

In Eq. (53), $E(\mathbf{x})$ is the energy at point $\mathbf{x}$ and E_0, $\mathbf{g}_0$, and $\mathbf{H}_0$ are the energy, gradient, and Hessian at the point $\mathbf{x}_0$. It is convenient to think of the MEP as a one-dimensional slice through the PES. Defining the parameter s, which is dependent on $\boldsymbol{x}$, as the arc length along this one-dimensional slice gives rise to another Taylor series.

$$\mathbf{x}(s) = \mathbf{x}(0) + \boldsymbol{\nu}^0(0)s + \frac{1}{2}\boldsymbol{\nu}^1(0)s^2 + \frac{1}{6}\boldsymbol{\nu}^2(0)s^2 + \cdots \tag{54}$$

In Eq. (54), $\boldsymbol{\nu}^0$ and $\boldsymbol{\nu}^1$ are known as the tangent and curvature vectors. The tangent vector is given by

$$\boldsymbol{\nu}^0(s) = \frac{\mathrm{d}\mathbf{x}(s)}{\mathrm{d}s} = -\frac{\mathbf{g}(s)}{|\mathbf{g}(s)|} \tag{55}$$

Eq. (55) is the differential equation solved when following reaction paths. The curvature vector in Eq. (54) is given by

$$\boldsymbol{\nu}^1(s) = -\frac{\mathbf{H}\boldsymbol{\nu}^0 - (\boldsymbol{\nu}^{0t}\mathbf{H}\boldsymbol{\nu}^0)\boldsymbol{\nu}^0}{|\mathbf{g}(\mathbf{x})|} \tag{56}$$

The magnitude of the curvature, κ, is equal to the inverse of the radius of curvature, R

$$\kappa = |\boldsymbol{\nu}^1| = \frac{1}{R} \tag{57}$$

Large curvature indicates the reaction path is undergoing a tight turn, and small curvature corresponds to a shallow turn.

At the TS, where the gradient is zero, Eqs. (55) and (56) become ill defined and the tangent is equal to the Hessian eigenvector corresponding to the negative eigenvalue—this eigenvector is known as the transition vector. The curvature at the TS is given by

$$\boldsymbol{\nu}^1(s) = -[\mathbf{H}\boldsymbol{\nu}^0 - (\boldsymbol{\nu}^{0t}\mathbf{H}\boldsymbol{\nu}^0)\mathbf{I}]^{-1}[\mathbf{F}^1\boldsymbol{\nu}^0 - (\boldsymbol{\nu}^{0t}\mathbf{F}^1\boldsymbol{\nu}^0)\boldsymbol{\nu}^0] \tag{58}$$

where

$$\mathbf{F}_{ij}^{1} = \sum_{k} \mathbf{F}_{ijk} \boldsymbol{\nu}_{k}^{0} \tag{59}$$

Since the MEP is defined by an ordinary differential equation (ODE), standard numerical integration techniques can be used. The basic idea behind any numerical integration algorithm is to rewrite $\mathrm{d}\mathbf{x}$ and $\mathrm{d}s$ as $\Delta\mathbf{x}$ and Δs. In this way, the solution to Eq. (55) is given by a discrete set of points, $\{\mathbf{x}_i\}$, which are found by 'stepping' along the path with a step size of Δs. Although Eq. (55) appears to be rather benign, it can display stiff behavior [206] and be difficult to solve, especially in the regions where the gradient is very small. Therefore, solving Eq. (55) requires special care, and a number of specialized methods have been developed and reviewed in the literature [10,23,24,72, 128,177,178,207–217]. Generally speaking, numerical methods for integrating ODEs are classified as either explicit or implicit. Explicit methods use only information at the current point to define the position at the next point, while implicit methods use additional information from the next point, which typically means that these methods include some sort of iterative algorithm to converge the end point of each step.

Because the integration is numerical, different integration schemes yield different degrees of accuracy (i.e. the proximity of the points to the true MEP). The accuracy of a numerical integrator is defined by an order (i.e. first order, second order, etc.). The order of the integrator gives the highest order term in the Taylor expansion of the true solution. Hence, first-order methods give the correct first-order term in Eq. (54), second-order methods give correct first- and second-order terms in Eq. (54), and so on.

In the following sections, we describe some common methods for solving the reaction path equation and also discuss some interesting features and properties of MEPs. In Section 10.5.1, first-order methods are described. Included in the discussion are the explicit Euler integrator and its implicit and stabilized versions [212,213,216]. Second-order methods are considered in Section 10.5.2. There, we focus on the local quadratic approximation (LQA) method [214,215], the second-order Gonzalez–Schlegel algorithm [177,178], and the Hessian based predictor–corrector integrator [177,178,210,211]. Higher order methods are considered in Section 10.5.3 [209,214]. Path following methods based on classical dynamics, known as dynamic reaction path (DRP) methods [218–221], are discussed in Section 10.5.4. Lastly, in Section 10.5.5, we have included some practical considerations and common troubleshooting tips related to reaction path following calculations.

10.5.1 First-order methods

Perhaps the simplest integrator (both conceptually and in terms of coding) is the Euler method. This method is correct only to the first-order term in Eq. (54) and gives the next point in the integration, $\mathbf{x}_{i+1}$, as

$$\mathbf{x}_{i+1} = \mathbf{x}_i - \frac{\mathbf{g}(\mathbf{x}_i)}{|\mathbf{g}(\mathbf{x}_i)|}\Delta s = \mathbf{x}_i + \boldsymbol{\nu}_i^0 \Delta s \tag{60}$$

In the limit of infinitesimally small step size, Euler integration yields the exact MEP. However, in practice Euler integration suffers from a number of pathologies. The steps taken in an Euler integration are linear, meaning that the Euler path will deviate from the true reaction path wherever the MEP is at all non-linear. Indeed, Euler integration is notorious for developing wild oscillations back and forth across the true solution for larger step sizes. This pathology is especially apparent in regions where the path curvature is large or where the slope along the path is small. As a result, reaction path following calculations using Euler integration must use very small steps. The problem, though, is that calculations using a small step size require a large number of energy and gradient evaluations (one energy and gradient evaluation is needed per step), which may be quite costly for moderate to large systems.

To combat this problem, Ishida, Morokuma, and Komornicki (IMK) developed the Euler stabilization (ES) algorithm [212]. The IMK algorithm is shown in Fig. 10.6a. Each ES step can be broken into two parts. First, an explicit Euler step, i.e. Eq. (60), is taken from $\mathbf{x}_i$ to $\mathbf{x}^*$, where the energy (E^*) and gradient ($\mathbf{g}^*$) are both evaluated. The second piece of ES is to stabilize the Euler step by minimizing the energy along the line bisecting the angle between ($\mathbf{x}_i - \mathbf{x}^*$) and $\mathbf{g}^*$. The minimum on the bisector is chosen as $\mathbf{x}_{i+1}$, and the next ES step starts from there. In cases where the angle between ($\mathbf{x}_i - \mathbf{x}^*$) and $\mathbf{g}^*$ is

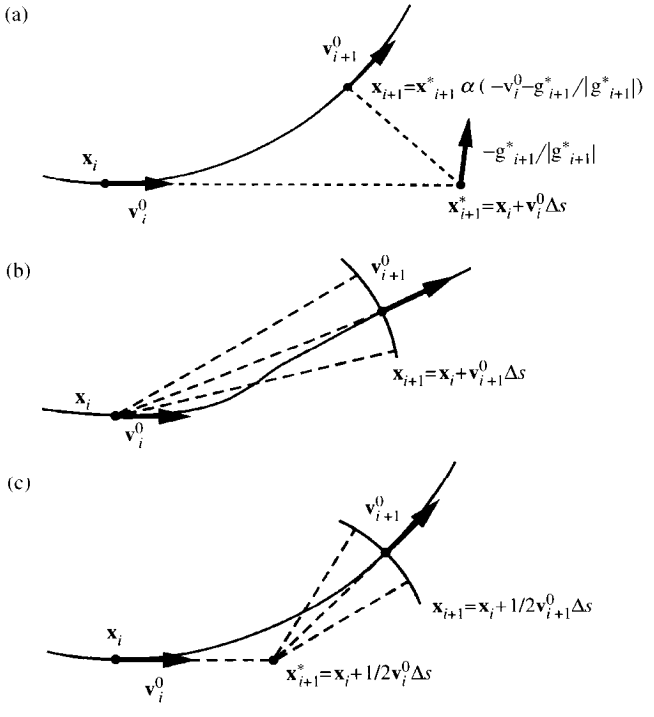

Fig. 10.6. Schematic representations of implicit reaction path following integrators: (a) Ishida, Morokuma, and Komornicki; (b) Müller–Brown; and (c) second-order Gonzalez and Schlegel (from Ref. [72] with permission).

nearly linear or when small step sizes are used, the stabilization step must be omitted. Although ES is much more stable than explicit Euler, difficult regions of the PES can still be problematic and cause oscillations in the ES pathway.

Another first-order method developed to overcome the problems of explicit Euler integration is the Müller–Brown (MB) method [213]. The MB method makes use of the implicit Euler integrator. Here, the step depends on the gradient at the endpoint, which is unknown. To find the endpoint of each step, a constrained optimization is required. The MB step begins with an explicit Euler step. Then, the energy is minimized according to the constraint that the distance between the starting and ending points remains constant

$$|\mathbf{x}_i - \mathbf{x}_{i+1}| = \Delta s \tag{61}$$

Fig. 10.6b shows, schematically, the MB method. The gradient at the endpoint after the constrained minimization will be parallel to the step direction, $(\mathbf{x}_i - \mathbf{x}_{i+1})$. Therefore, the MB step can be given by

$$\mathbf{x}_{i+1} = \mathbf{x}_i - \frac{\mathbf{g}_{i+1}}{|\mathbf{g}_{i+1}|}\Delta s = \mathbf{x}_i + \boldsymbol{\nu}_{i+1}^0 \Delta s \tag{62}$$

10.5.2 Second-order methods

Second-order methods have also been proposed in the literature for integrating MEPs. Although a standard numerical integrator, such as the second-order Runge–Kutta method, could be used, it is generally accepted that a more effective approach is to directly expand the PES as a second-order Taylor series. Truncating the Taylor series in Eq. (53) at the second-order term and differentiating gives

$$\mathbf{g}(\mathbf{x}) = \mathbf{g}_0 + \mathbf{H}_0 \Delta \mathbf{x} \tag{63}$$

Substituting Eq. (63) into Eq. (55) gives the LQA of Page and McIver [213–215], which is an explicit second-order integrator.

$$\frac{\mathrm{d}\mathbf{x}(s)}{\mathrm{d}s} = -\frac{\mathbf{g}_0 + \mathbf{H}_0 \Delta \mathbf{x}}{|\mathbf{g}_0 + \mathbf{H}_0 \Delta \mathbf{x}|} \tag{64}$$

In practice, Eq. (64) is integrated by parameterization and casting the problem in the Hessian eigenvector space. Sun and Ruedenberg [217] have modified the LQA algorithm by using each point, $\mathbf{x}_i$, as the midpoint in the integration range, rather than the endpoint.

Gonzalez and Schlegel developed an implicit second-order integrator for reaction path following (GS2) [177,178], which is shown in Fig. 10.6c. Each GS2 step consists of two components. First, an explicit Euler step of length $\frac{1}{2}\Delta s$ is taken from the current point, $\mathbf{x}_i$, to a pivot point, $\mathbf{x}^*$.

$$\mathbf{x}^* = \mathbf{x}_i + \frac{1}{2}\mathbf{v}_i^0 \Delta s \tag{65}$$

The second piece of a GS2 step begins by taking an additional step of length $\frac{1}{2}\Delta s$ from the pivot point to the end point, $\mathbf{x}_{i+1}$. The energy, $E(\mathbf{x}_{i+1})$, is minimized using QN under the constraint that

$$|\mathbf{x}_{i+1} - \mathbf{x}^*| = \frac{1}{2}\Delta s \tag{66}$$

At the end of the optimization, the component of the gradient perpendicular to $|\mathbf{x}_{i+1} - \mathbf{x}^*|$ is zero. Just as with the MB implicit integrator, the GS2 step can be written in terms of the tangent at the initial point, $\mathbf{x}_i$, and at the final point, $\mathbf{x}_{i+1}$.

$$\mathbf{x}_{i+1} = \mathbf{x}_i - \frac{1}{2}\frac{\mathbf{g}_i}{|\mathbf{g}_i|}\Delta s - \frac{1}{2}\frac{\mathbf{g}_{i+1}}{|\mathbf{g}_{i+1}|}\Delta s = \mathbf{x}_i + \frac{1}{2}\boldsymbol{\nu}_i^0\Delta s + \frac{1}{2}\boldsymbol{\nu}_{i+1}^0\Delta s \tag{67}$$

Eq. (67) is similar to the implicit trapezoid approach for integrating stiff differential equations, except that the GS2 method utilizes optimization to obtain $\mathbf{x}_{i+1}$. It should be noted that no energy or derivative calculations are necessary at the pivot point. Furthermore, since

$$|\mathbf{x}^* - \mathbf{x}_i| = |\mathbf{x}_{i+1} - \mathbf{x}^*| = \frac{1}{2}\Delta s \tag{68}$$

the points $\mathbf{x}_i$, $\mathbf{x}^*$, and $\mathbf{x}_{i+1}$ form an isosceles triangle. By construction, two tangents to a circle form an isosceles triangle. Therefore, the GS2 algorithm will follow an arc of a circle exactly.

Recently, Hratchian and Schlegel (HS) introduced a second-order predictor–corrector reaction path following integrator [210,211]. A related algorithm has also been used for integrating *ab initio* classical trajectories [222,223]. Predictor–corrector integrators, as their name suggests, couple two different integration methods. The predictor integrator moves from the current point, $\mathbf{x}_i$, to a guess for the next point, $\mathbf{x}_{i+1}$. Using information (e.g. energy and/or derivatives) at the predicted $\mathbf{x}_{i+1}$, the corrector integrator re-integrates over the same interval and refines, or corrects, $\mathbf{x}_{i+1}$. The basic idea is illustrated in Fig. 10.7. The HS method uses LQA for the predictor step and a modified Bulirsch–Stoer integrator [206,224–227] for the corrector step. The corrector step increases the stability of LQA and allows for large steps without loosing accuracy. Bulirsch–Stoer integration requires several gradient evaluations per step, which would make direct use with electronic structure methods quite costly. To overcome this bottleneck, the HS integrator uses the positions, energies, gradients, and Hessians at $\mathbf{x}_i$ and the predicted point, $\mathbf{x}_{i+1}$, to construct a local analytic surface. The Bulirsch–Stoer corrector integration is carried out on this fitted surface. Relative to the cost of electronic structure energy and derivative

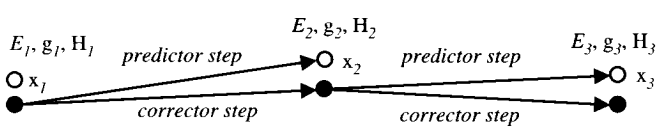

Fig. 10.7. Schematic representation of predictor–corrector integration, such as the integrator used in the Hratchian–Schlegel method (from Ref. [223] with permission).

calculations, energy and gradient evaluations on the fitted surface are free and the corrector step adds a negligible cost to the standard LQA calculation, which is more than compensated for by the larger step sizes that the HS algorithm allows. In the current implementation, HS fits the LQA data to a distance weighted interpolant surface for the corrector integration [228–231]. The energy on this surface, E_{DWI}, is given by

$$E_{\mathrm{DWI}} = w_i T_i + w_{i+1} T_{i+1} \tag{69}$$

where T_i and T_{i+1} are Taylor expansions about $\mathbf{x}_i$ and $\mathbf{x}_{i+1}$, respectively. These Taylor expansions,

$$\begin{aligned} T_i(\mathbf{x}) &= E_i + \mathbf{g}_i^{\mathrm{t}}(\mathbf{x} - \mathbf{x}_i) + \frac{1}{2}(\mathbf{x} - \mathbf{x}_i)^{\mathrm{t}}\mathbf{H}_i(\mathbf{x} - \mathbf{x}_i), \\ T_{i+1}(\mathbf{x}) &= E_{i+1} + \mathbf{g}_{i+1}^{\mathrm{t}}(\mathbf{x} - \mathbf{x}_{i+1}) + \frac{1}{2}(\mathbf{x} - \mathbf{x}_{i+1})^{\mathrm{t}}\mathbf{H}_i(\mathbf{x} - \mathbf{x}_{i+1}) \end{aligned} \tag{70}$$

are weighted by w_i and w_{i+1},

$$w_i = \frac{|(\mathbf{x} - \mathbf{x}_i)|^2}{|(\mathbf{x} - \mathbf{x}_i)|^2 + |(\mathbf{x} - \mathbf{x}_i)|^2}, \qquad w_{i+1} = \frac{|(\mathbf{x} - \mathbf{x}_{i+1})|^2}{|(\mathbf{x} - \mathbf{x}_{i+1})|^2 + |(\mathbf{x} - \mathbf{x}_{i+1})|^2} \tag{71}$$

The LQA and HS methods require second derivatives. Although the GS2 equations do not explicitly require the Hessian, second derivatives are used for the constrained optimization step. For the same reasons we discussed in Section 10.3.5.4, the calculation of second derivatives can greatly increase the cost of a reaction path following calculation and limit the usefulness of these methods for the study of moderate and large chemical systems. As before, Hessian updating can be employed, and previous studies have shown that Hessian updating is a viable option for reaction path following using these second-order integration schemes [177,211,232]. Also noteworthy is that Hessian updating methods designed for minimization cannot be used with reaction path following since the formulas for most of those updates become ill conditioned when the Hessian has one or more negative eigenvalues [129]. Recall that the same concern was encountered in our earlier discussion of TS optimization. Therefore, Hessian updating methods developed for TS optimization are also useful in reaction path following (i.e. MS, PSB, Bofill, etc.).

10.5.3 Higher order integrators

Higher order methods can also be envisioned. Here, we provide only a brief discussion of two sets of higher order integrators, since they are not often used in connection with electronic structure calculations. The first set of these methods, developed by Page et al. [214], consists of two explicit third-order integrators. One of these integrators finds each point on the reaction path by directly solving the first four terms of Eq. (54). The PES third derivatives are required for $\boldsymbol{\nu}^2$, which can either be computed analytically or numerically. A similar method provides a third-order analogue to LQA, the CLQA algorithm. After each LQA step, the Hessians at the initial and final points can be used

to estimate $\boldsymbol{\nu}^2$ by finite difference by recognizing that $\boldsymbol{\nu}^2$ depends on the derivative of the force constants with respect to the arc length, s.

Gonzalez and Schlegel [209] have also developed a series of third- and fourth-order methods. All of their higher order approaches use implicit integrators and are extensions of the GS2 algorithm. One of these, a fourth-order method, uses the tangent and curvature vectors at the initial and final points of each step.

$$\mathbf{x}_{i+1} = \mathbf{x}_i + \frac{1}{2}\boldsymbol{\nu}_i^0 \Delta s + \frac{1}{2}\boldsymbol{\nu}_{i+1}^0 \Delta s + \frac{1}{12}\boldsymbol{\nu}_i^1 \Delta s^2 - \frac{1}{12}\boldsymbol{\nu}_{i+1}^1 \Delta s^2 \tag{72}$$

10.5.4 Dynamic reaction path

The solution for the MEP, as shown above, is time independent. Of course, molecular systems exist in a time dependent universe and they are constantly exercising motions on the PES different than the specific motion described by the MEP. An alternative picture for the reaction path is to allow the nuclei to move on the PES according to Newton's equations of motion. In terms of time, the coordinates of the system at time t_i, $\mathbf{x}_i$, can be given by the Taylor expansion

$$\mathbf{x}_i = \mathbf{x}_{i-1} + \mathbf{v}_{i-1}\Delta t + \frac{1}{2}\mathbf{a}_{i-1}\Delta t^2 + \cdots \tag{73}$$

where $\mathbf{v}$ and $\mathbf{a}$ are velocity and acceleration, respectively. The velocity is given by a similar Taylor series,

$$\mathbf{v}_i = \mathbf{v}_{i-1} + \mathbf{a}_{i-1}\Delta t + \cdots \tag{74}$$

and the acceleration is given by

$$\mathbf{F} = \mathbf{ma}$$

where $\mathbf{m}$ is a diagonal matrix of atomic masses and

$$\mathbf{F} = -\frac{\mathrm{d}V}{\mathrm{d}\mathbf{x}} = -\mathbf{g} \tag{75}$$

where V is the potential energy of the system, which is given by the value of PES. For the case where infinitesimal steps in t are taken and the kinetic energy is completely removed, or damped, from the system at every step, the path mapped out by classical dynamics (beginning at the TS) is identical to the IRC.

Starting at the TS and following a time-dependent path according to Newton's equation of motion yields the DRP of Stewart et al. [221]. Since a DRP without removing any kinetic energy is the same as a classical trajectory calculation, it can be used to study energy transfer processes during the course of a reaction, and understand how the energy in specific modes behaves relative to the reaction coordinate, or IRC [220]. By damping the kinetic energy at each step one can use the DRP as a means for finding qualitative MEPs. This is especially useful where the purpose for finding the MEP is to ensure that a located TS lies on a pathway connecting specific PES minima, and has been shown to be an efficient alternative to conventional integration of the MEP (i.e. using methods

discussed in Sections 10.5.2 and 10.5.3). We have developed a method called damped velocity Verlet (DVV) that controls the path accuracy by employing a variable step size, Δt [219]. The DVV step size control is based on the third-order error scaling of velocity Verlet. Given the current step size of Δt_i and desired error in the path, Δ_0, the next step size, Δt_{i+1}, is set according to

$$\Delta t_{i+1} = \Delta t_i \left| \frac{\Delta_0}{\Delta_i} \right|^{1/3} \tag{76}$$

In Eq. (76) Δ_i is an estimated error in the path at step i. This estimated error is shown schematically in Fig. 10.8, and is obtained by propagating a double sized step from $\mathbf{x}_{i-2}$ to $\mathbf{x}_i'$ and comparing this to the point $\mathbf{x}_i$.

10.5.5 Practical considerations

We conclude Section 10.5 by discussing a few practical points related to reaction path following. This section begins with tips for choosing an appropriate reaction path following algorithm based on the application at hand. Projected frequencies and the relationship between path accuracy and errors in the path's tangent, curvature, and projected frequencies are considered in the second subsection. The third subsection is concerned with bifurcations, which are novel topological features of PESs and reaction paths. In the last subsection we suggest steps for difficult reaction path calculations.

10.5.5.1 Algorithm choice

We begin this section by briefly outlining some of the key points that need to be considered when choosing an algorithm for a reaction path following calculation. As mentioned earlier, reaction path following is typically employed to ensure that an optimized TS lies on a MEP connecting the correct reactant and product minima and/or to accurately determine reaction rates. These two applications of reaction path following calculations have different requirements on the quality and efficiency of the integration. In the former case, efficiency has primacy over strict accuracy, although it is essential that the MEP integration be trustworthy and able to qualitatively follow the true pathway. In the latter case, efficiency is desirable, but the accuracy of the path is paramount (see Section 10.5.5.2).

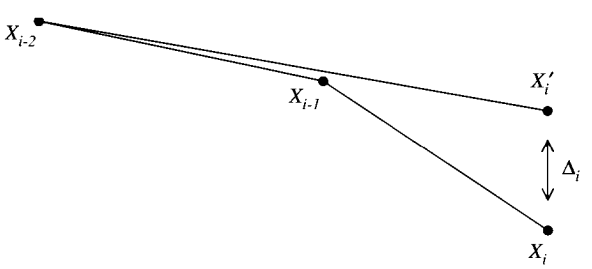

Fig. 10.8. Graphical depiction of damped velocity Verlet (DVV) path error estimation used for time variation (from Ref. [219] with permission).

First, we consider the ability of the various integrators discussed above to provide accurate pathways, such as those required for VTST and RPH calculations. DRP methods are not appropriate for these applications of reaction path following since they provide only an approximate path. A comparison of the accuracy of multiple integrators has been provided in a series of papers by Truhlar and coworkers [207,208,233]. Schlegel and colleagues have also provided comparisons of the accuracy afforded by a series of typical first- and higher-order integrators [209,234]. Fig. 10.9 shows results of reaction path following using a number of first- and second-order methods on the Müller–Brown surface. A step size of 0.2 has been used for all of the integrations shown. The solid line is the MEP computed by Euler integration using a very small step size (0.0001). The portion of the MEP considered in this example connects the TS at (−0.822, 0.624) and the minimum at (−0.558, 1.442). Because the reaction path is curved, this surface can be challenging for reaction path following integrators. It is clear from the figure that the first-order methods deviate most from the true MEP while the second-order methods perform very well. The accuracy of the first-order methods can be improved by decreasing the step size, but this option is undesirable since it means an increased number of energy and derivative evaluations. On the other hand, most second- and higher-order methods, such as LQA, CLQA, and HS, all require second derivatives that are often more expensive than multiple energy and gradient calculations, but this characteristic may not represent a bottleneck if the MEP is being determined for subsequent rate constant calculations since

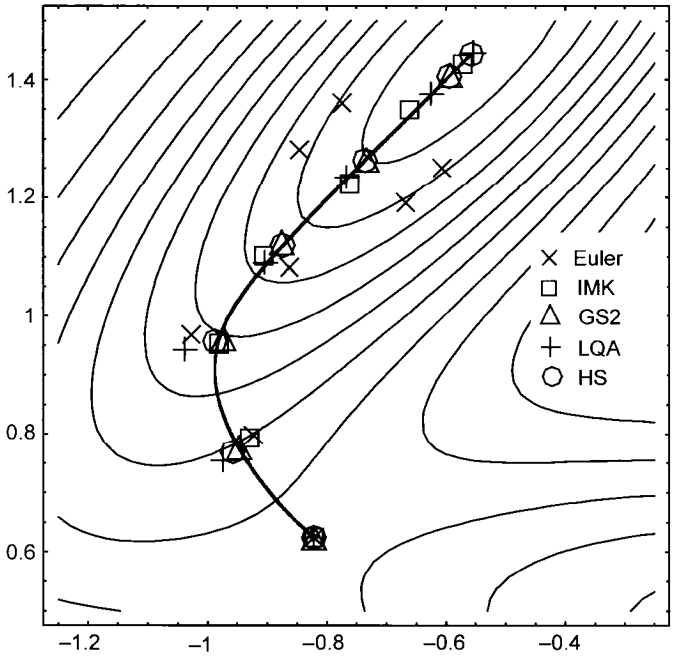

Fig. 10.9. Reaction path following on the Müller–Brown surface using Euler, Ishida, Morokuma, and Komornicki (IMK), local quadratic approximation (LQA), Hratchian–Schlegel (HS), and second-order Gonzalez–Schlegel (GS2) methods.

VTST and RPH calculations also require Hessians along the MEP. Formally, the GS2 method does not require second derivatives. However, in practice the constrained optimization at the end of each step uses Newton minimization and requires a Hessian matrix. Although updated Hessians can be used with GS2, it has been shown[234] that analytic Hessians are useful in providing very accurate pathways. One particularly advantageous feature of GS2 over LQA and CLQA is that larger steps can be used to give similar error in the path since GS2 is an implicit method. Additionally, the implicit nature of GS2 makes it much more stable and robust along flat PESs and in regions of the MEP where the gradient is small. This is especially important near the TS. Although this result makes GS2 an attractive method for accurate path following, the integration can be somewhat expensive due to the constrained optimizations, which typically require three or four cycles per step. The HS method is also able to accurately follow the MEP in difficult regions of the path, and only requires one evaluation of the energy and derivatives per step.

If reaction path following is used to confirm a TS lies on a pathway connecting appropriate reactant and product minima, the approaches used for kinetics studies are more expensive than the nature of the application demands. For qualitative path following, first-order methods are still not preferred since they require very small steps and consequently progress down the MEP relatively slowly. To make second-order methods more tractable for large systems Hessian updating can be employed [177,211, 232]. The use of updated Hessians only requires a slight decrease in the step size. As a result, methods such as LQA, CLQA, GS2, and HS progress down the MEP faster than the first-order approaches since they are able to take larger steps. To demonstrate the applicability of Hessian updating to reaction path following integrators requiring force constant matrices we have included Table 10.7, which shows the perpendicular distance between points on a path computed with the HS integrator using all analytic Hessians and using all updated Hessians. From this data, it is clear that Hessian updating can lead to qualitatively good pathways. DRP approaches are efficient methods for elucidating qualitative reaction pathways. Although these methods are able to take moderate step sizes, methods such as LQA, GS2, and HS are able to take considerably larger steps. The DVV method, which uses a dynamic time step, requires more integration steps than GS2,

Table 10.7 RMS errors in position (Å) for HS reaction path following Hessian updating[a,b]

Reaction	Step size (bohr)	RMS error
$HNC \rightarrow HCN$	0.10	3.05×10^{-4}
	0.40	1.05×10^{-2}
$CH_3CH_2F \rightarrow CH_2CH_2 + HF$	0.10	4.73×10^{-3}
	0.40	8.46×10^{-2}
$ClCH_3 + Cl^- \rightarrow Cl^- + CH_3Cl$	0.10	3.04×10^{-3}
	0.40	3.46×10^{-2}
Diels–Alder	0.10	1.58×10^{-2}
	0.40	9.50×10^{-2}

[a]For complete details see Ref. [211].
[b]Bofill's updating scheme for transition state optimization has been employed.

Table 10.8 Comparison of the number of Fock matrix evaluations for damped velocity Verlet and second-order Gonzalez–Schlegel reaction path following[a]

Reaction	Fock evaluations for DVV[b]	Fock evaluations for GS2[c]
$CH_3 + HF \rightarrow CH_4 + F$	1276	716
$CH_2OH \rightarrow CH_3O$	1236	668
Diels–Alder reaction	2142	1352
$CH_3CH_2F \rightarrow CH_2CH_2 + HF$	1439	4281
Ene reaction	2134	7406
$[Ir(CO)_2I_3(CH_3)]^- \rightarrow [Ir(CO)I_3(COCH_3)]^-$	1078	9579

[a]For complete details see Ref. [219].
[b]DVV calculations were run with a damping factor of 0.04 au/fs.
[c]GS2 calculations were run with a step size of 0.1 $amu^{1/2}$ bohr.

but becomes more efficient because it is an explicit method and does not require constrained optimizations at each step. Table 10.8 shows the total number of Fock matrix evaluations, which is the bottleneck for large systems, necessary to follow a series of reaction paths using DVV and GS2 methods. The data clearly indicates that DVV is more efficient than GS2.

10.5.5.2 Projected frequencies and coupling matrix elements

As mentioned earlier, MEPs can be used to compute reaction rates using VTST or RPH methods. In order to use either of these approaches it is necessary to compute the vibrational frequencies lying perpendicular to the MEP [234]. The perpendicular vibrational frequencies are determined by projecting out motion along the tangent, $\boldsymbol{\nu}^0$, from the Hessian and then calculating the projected frequencies according to the normal procedures [235]. Mathematically, the projected Hessian, $\tilde{\mathbf{H}}$, is given by

$$\tilde{\mathbf{H}} = \mathbf{PHP} \tag{77}$$

where the projector, $\mathbf{P}$, is

$$\mathbf{P} = \mathbf{I} - \boldsymbol{\nu}^0\boldsymbol{\nu}^{0t} \tag{78}$$

If the calculation is carried out in mass-weighted Cartesian coordinates then overall translation and rotation are also projected out of the Hessian.

Reaction rate calculations also require the coupling matrix terms $\mathbf{B}$. The vector $\mathbf{B}$ indicates the coupling between motion along the reaction path and the normal modes of vibration corresponding to the projected frequencies, i.e. the normal modes that are perpendicular to the MEP. The ith element of $\mathbf{B}$ is

$$\mathbf{B}_i = \boldsymbol{\nu}^{0t}\frac{d\mathbf{L}_i}{ds} = -\boldsymbol{\nu}^{1t}\mathbf{L}_i \tag{79}$$

where $\mathbf{L}_i$ is the ith eigenvector of $\tilde{\mathbf{H}}$. In order to compute reliable projected frequencies and coupling matrix elements, it is necessary to integrate the MEP accurately. This is especially important in the region very near the TS where the gradient is very small. Precise MEPs are also required for accurate projected frequencies and coupling matrix

elements in regions where the valley has steep walls since small displacements from the MEP can cause large errors in the tangent and curvature vectors.

10.5.5.3 Bifurcation

Bifurcation is a novel topological feature that can be present on a PES [236], which occurs when one valley branches into two. More specifically, bifurcation can occur as a valley progresses down the MEP from the TS and splits into two different minima, or as a valley rises from a minimum and splits into two different MEPs heading toward two different TSs. Along the reaction path of a simple valley, all of the projected frequencies will be real. This corresponds to all of the eigenvalues of the projected Hessian being positive. If one or more of the projected frequencies are imaginary, this indicates that the PES is a maximum perpendicular to the reaction path and the path lies on a ridge. The development of the ridge is marked by a valley-ridge inflection (VRI) point. At the VRI point one projected frequency is zero. On one side of the VRI point this projected frequency is real and on the other side it is imaginary. Fig. 10.1 shows a model PES that has a VRI point on the MEP leading from Transition State B. At the VRI point the MEP integration is displaced slightly (along the Hessian eigenvector with a corresponding eigenvalue of zero) leading to the branching displayed in the figure. Bifurcation and methods for locating VRI points are active areas of research, and interested readers are referred to the current literature for more detailed discussion [156,158,236–251].

10.5.5.4 Tips for difficult reaction path calculations

In this subsection we offer suggestions for difficult reaction path following calculations. In conjunction with suggestions for correcting problems, we describe some useful diagnostics. Testing these diagnostics is especially important for calculations that terminate improperly (e.g. an SCF failure is encountered, etc.). Our principle focus here is on calculations where reaction path following is employed to ensure that an optimized TS lies on a pathway connecting the appropriate reactant and product minima. For situations where the primary concern is a very accurate path for determining reaction rates, these suggestions may also be useful.

The first test is to generate a plot of energy *vs.* reaction coordinate. This plot should be smooth and show a monotonic decrease in energy as the reaction path progresses from the TS to the reactant and product minima. A second diagnostic is to plot the r.m.s. force *vs.* reaction coordinate. This plot should show zero force at the TS and an increasing r.m.s. force for part of the progression to the minimum. Before reaching the minimum, the r.m.s. force will reach a maximum and begin to decrease until it goes to zero when the minimum is reached. Sharp spikes or sudden drops in either of these plots can indicate problems with the level of theory being used to study the chemistry under investigation. Mild undulations in either plot can indicate a problem with the actual integration of the MEP. In many cases, this problem can be corrected by taking smaller steps. If a first-order method is being used, an alternative solution is to switch to a second-order integrator.

For predictor–corrector and implicit integrators, the accuracy of the path can often be enhanced by tightening convergence criteria. Of the methods discussed in this chapter, this approach is applicable for MB, GS2, and HS. MB and GS2 both employ constrained optimizations to determine the tangent at the endpoint of each step. In the practical

implementation of the constrained optimization the accuracy of the endpoint is based on convergence criteria, which can be tightened. In the case of HS, the Bulirsch–Stoer corrector step repeats the integration of the MEP with decreasing step size until an extrapolation to zero step size can be made with an estimated error in the energy below a threshold. Decreasing this acceptance threshold can lead to a more accurate integration by the HS algorithm.

DVV pathways can also display energy and force oscillations. This pathology can usually be corrected by modifying the various parameters involved in the calculation. Specifically, smaller ν_0 and Δ_0 values can lead to DVV paths more closely resembling the actual MEP. In fact, Andersen and Carter [252,253] have used values for these parameters that are much more stringent than those originally proposed. Note, though, that small values for either parameter will require more points along the MEP to progress to the minima, leading to more gradient evaluations and longer calculation times.

10.6 SUMMARY AND OUTLOOK

In this chapter, we have provided an overview of the current status of local minimization, transition state optimization, and reaction path following using electronic structure methods. This review also offered a number of suggestions for overcoming difficulties commonly encountered in geometry optimization and reaction path following. Clearly, great progress has been made in these areas in the past 40 years; however, the work is far from complete. Indeed, the development of new methods for exploring *ab initio* PES continues to be an active area of research in the computational quantum chemistry community, especially within the context of hybrid methods (i.e. QM/MM and QM/QM) and the study of very large systems.

In recent decades, electronic structure methods were used to study an ever-increasing diversity of chemistries ranging in size from a few atoms to thousands of nuclei. Doubtless, the future will bring faster computers and more efficient energy algorithms that will expand the limits of computational chemistry beyond the fringes of today's most optimistic estimates. As we have shown here, tools for exploring PES are invaluable and developments in this area will continue to respond to the demand for minimization algorithms featuring fast convergence, robust transition state optimization techniques, and reaction path following integrators coupling accuracy with efficiency.

10.7 REFERENCES

1 J.I. Steinfeld, J.S. Francisco and W.L. Hase, Chemical kinetics and dynamics, Prentice-Hall, Upper Saddle River, NJ, 1999.
2 S. Glasstone, K.J. Laidler and H. Eyring, The theory of rate processes; the kinetics of chemical reactions, viscosity, diffusion and electrochemical phenomena, McGraw-Hill, New York, 1941.
3 D.G. Truhlar and B.C. Garrett, Annu. Rev. Phys. Chem., 35 (1984) 159–189.
4 D.G. Truhlar, B.C. Garrett and S.J. Klippenstein, J. Phys. Chem., 100 (1996) 12771–12800.
5 B.C. Garrett and D.G. Truhlar, in Encyclopedia of computational chemistry, P.v.R. Schleyer, N.L. Allinger, T. Clark, J. Gasteiger, P.A. Kollman, H.F. Schaefer III and P.R. Schreiner, (Eds.), Wiley, Chichester, 1998, p. 3094–104.

6 W.H. Miller, N.C. Handy and J.E. Adams, J. Chem. Phys., 72 (1980) 99–112.
7 E. Kraka, in Encyclopedia of computational chemistry, P.v.R. Schleyer, N.L. Allinger, T. Clark, J. Gasteiger, P.A. Kollman, H.F. Schaefer III and P.R. Schreiner, (Eds.), Wiley, Chichester, 1998, p. 2437–63.
8 P. Pulay, in: D.R. Yarkony (Ed.), Modern electronic structure theory, World Scientific, Singapore, 1995, p. 1191.
9 H.B. Schlegel, in Encyclopedia of computational chemistry, P.v.R. Schleyer, N.L. Allinger, T. Clark, J. Gasteiger, P.A. Kollman, H.F. Schaefer III and P.R. Schreiner, (Eds.), Wiley, Chichester, 1998, pp. 1136–42.
10 H.B. Schlegel, in Encyclopedia of computational chemistry, P.v.R. Schleyer, N.L. Allinger, T. Clark, J. Gasteiger, P.A. Kollman, H.F. Schaefer III, and P.R. Schreiner, (Eds.), Wiley, Chichester, 1998, pp. 2432–37.
11 G. Henkelman, G. Jóhannesson and H. Jónsson, in: S.D. Schwartz (Ed.), Progress on theoretical chemistry and physics, Kluwer, Dordrecht, 2000.
12 F. Jensen, in Encyclopedia of computational chemistry, P.v.R. Schleyer, N.L. Allinger, T. Clark, J. Gasteiger, P.A. Kollman, H.F. Schaefer III, and P.R. Schreiner, (Eds.), Wiley, Chichester, 1998, pp. 3114–23.
13 C.A. Floudas and P.M. Pardalos, State of the art in global optimization: Computational methods and applications, Kluwer, Dordrecht, 1996.
14 C.A. Floudas and P.M. Pardalos, Optimization in computational chemistry and molecular biology: Local and global approaches, Kluwer, Dordrecht, 2000.
15 R. Horst and P.M. Pardalos, Handbook of global optimization, Kluwer, Dordrecht, 1995.
16 R. Horst, P.M. Pardalos and N.V. Thoai, Introduction to global optimization, Kluwer, Dordrecht, 2000.
17 A. Törn and A. Zhilinskas, Global optimization, Springer, Berlin, 1989.
18 M. Ben-Nun and T.J. Martinez, Adv. Chem. Phys., 121 (2002) 439–512.
19 G.A. Voth, J. Phys. Chem. A, 103 (1999) 9383.
20 R. Kosloff, Annu. Rev. Phys. Chem., 45 (1994) 145–178.
21 D. Heidrich, The reaction path in chemistry: Current approaches and perspectives, Kluwer, Dordrecht, 1995.
22 D. Heidrich, W. Kliesch and W. Quapp, Properties of chemically interesting potential energy surfaces, Springer, Berlin, 1991.
23 M.A. Collins, Adv. Chem. Phys., 93 (1996) 389–453.
24 M.L. McKee and M. Page, in: K.B. Lipkowitz, D.B. Boyd (Eds.), Reviews in computational chemistry, VCH, New York, NY, 1993, pp. 35–65.
25 D.J. Wales, Energy landscapes, Cambridge University Press, Cambridge, 2003.
26 J. Simons and J. Nichols, Int. J. Quantum Chem., Suppl. 24 (1990) 263–276.
27 C.E. Dykstra, Ab initio calculation of the structures and properties of molecules, Elsevier, Amsterdam, 1988.
28 P. Jørgensen, J. Simons and North Atlantic Treaty Organization, Scientific Affairs Division, Geometrical derivatives of energy surfaces and molecular properties, Reidel, Dordrecht, 1986.
29 F. Jensen, Introduction to computational chemistry, Wiley, Chichester, 1999.
30 X.S. Li, J.M. Millam, G.E. Scuseria, M.J. Frisch and H.B. Schlegel, J. Chem. Phys., 119 (2003) 7651–7658.
31 K.N. Kudin, G.E. Scuseria and E. Cances, J. Chem. Phys., 116 (2002) 8255–8261.
32 S. Goedecker, Rev. Mod. Phys., 71 (1999) 1085–1123.
33 G.E. Scuseria, J. Phys. Chem. A, 103 (1999) 4782–4790.
34 J.M. Millam and G.E. Scuseria, J. Chem. Phys., 106 (1997) 5569–5577.
35 W.Z. Liang and M. Head-Gordon, J. Chem. Phys., 120 (2004) 10379–10384.
36 Y. Shao, C. Saravanan, M. Head-Gordon and C.A. White, J. Chem. Phys., 118 (2003) 6144–6151.
37 D.R. Bowler, T. Miyazaki and M.J. Gillan, J. Phys.-Condens. Matter, 14 (2002) 2781–2798.
38 M.C. Strain, G.E. Scuseria and M.J. Frisch, Science, 271 (1996) 51–53.
39 P. Pulay, Mol. Phys., 17 (1969) 197–204.
40 K. Thompsen and P. Swanstron, Mol. Phys., 26 (1973) 735.

41 J.A. Pople, R. Krishnan, H.B. Schlegel and J.S. Binkley, Int. J. Quantum Chem. Quantum Chem. Symp., 13 (1979) 225–241.
42 J.D. Augspurger and C.E. Dykstra, J. Phys. Chem., 95 (1991) 9230–9238.
43 P.E. Maslen, D. Jayatilaka, S.M. Colwell, R.D. Amos and N.C. Handy, J. Chem. Phys., 95 (1991) 7409–7417.
44 S.M. Colwell, D. Jayatilaka, P.E. Maslen, R.D. Amos and N.C. Handy, Int. J. Quantum Chem., 40 (1991) 179–199.
45 J.F. Gaw, Y. Yamaguchi, H.F. Schaefer and N.C. Handy, J. Chem. Phys., 85 (1986) 5132–5142.
46 J.F. Gaw, Y. Yamaguchi and H.F. Schaefer, J. Chem. Phys., 81 (1984) 6395–6396.
47 P. Pulay, J. Chem. Phys., 78 (1983) 5043–5051.
48 P. Pulay, G. Fogarasi, F. Pang and J.E. Boggs, J. Am. Chem. Soc., 101 (1979) 2550.
49 P. Pulay and G. Fogarasi, J. Chem. Phys., 96 (1992) 2856–2860.
50 G. Fogarasi, X.F. Zhou, P.W. Taylor and P. Pulay, J. Am. Chem. Soc., 114 (1992) 8191–8201.
51 J. Baker, J. Comput. Chem., 14 (1993) 1085–1100.
52 C.Y. Peng, P.Y. Ayala, H.B. Schlegel and M.J. Frisch, J. Comput. Chem., 17 (1996) 49–56.
53 J. Baker, A. Kessi and B. Delley, J. Chem. Phys., 105 (1996) 192–212.
54 M. von Arnim and R. Ahlrichs, J. Chem. Phys., 111 (1999) 9183–9190.
55 K.N. Kudin, G.E. Scuseria and H.B. Schlegel, J. Chem. Phys., 114 (2001) 2919–2923.
56 K. Nemeth, O. Coulaud, G. Monard and J.G. Angyan, J. Chem. Phys., 113 (2000) 5598–5603.
57 Ö. Farkas and H.B. Schlegel, J. Chem. Phys., 109 (1998) 7100–7104.
58 Ö. Farkas and H.B. Schlegel, J. Chem. Phys., 111 (1999) 10806–10814.
59 B. Paizs, G. Fogarasi and P. Pulay, J. Chem. Phys., 109 (1998) 6571–6576.
60 B. Paizs, J. Baker, S. Suhai and P. Pulay, J. Chem. Phys., 113 (2000) 6566–6572.
61 K. Nemeth, O. Coulaud, G. Monard and J.G. Angyan, J. Chem. Phys., 114 (2001) 9747–9753.
62 S.R. Billeter, A.J. Turner and W. Thiel, Phys. Chem. Chem. Phys., 2 (2000) 2177–2186.
63 J. Baker, D. Kinghorn and P. Pulay, J. Chem. Phys., 110 (1999) 4986–4991.
64 X. Prat-Resina, M. Garcia-Viloca, G. Monard, A. Gonzalez-Lafont, J.M. Lluch, J.M. Bofill and J.M. Anglada, Theor. Chem. Acc., 107 (2002) 147–153.
65 T. Schlick and M. Overton, J. Comput. Chem., 8 (1987) 1025–1039.
66 T. Schlick, B.E. Hingerty, C.S. Peskin, M.L. Overton and S. Broyde, in: D.L. Beveridge, R. Lavery (Eds.), Theoretical biochemistry and molecular biophysics, Adenine Press, Schenectady, NY, 1991, pp. 39–58.
67 P. Derreumaux, G.H. Zhang, T. Schlick and B. Brooks, J. Comput. Chem., 15 (1994) 532–552.
68 R. Fletcher, Practical methods of optimization, Wiley, Chichester, 1987.
69 P.E. Gill, W. Murray and M.H. Wright, Practical optimization, Academic Press, New York, 1981.
70 J.E. Dennis and R.B. Schnabel, Numerical methods for unconstrained optimization and nonlinear equations, Prentice-Hall, Englewood Cliffs, NJ, 1983.
71 L.E. Scales, Introduction to non-linear optimization, Springer, New York, 1985.
72 H.B. Schlegel, in: D.R. Yarkony (Ed.), Modern electronic structure theory, World Scientific, Singapore, 1995, pp. 459–500.
73 D.F. Shanno, Math. Comput., 24 (1970) 647.
74 D. Goldfarb, Math. Comput., 24 (1970) 23.
75 R. Fletcher, Comput. J., 13 (1970) 317.
76 C.G. Broyden, J. Inst. Math. Appl., 6 (1970) 76.
77 M.J. Powell, Math. Program., 15 (1971) 1.
78 B.A. Murtagh and R.W.H. Sargent, Comput. J., 13 (1972) 185.
79 J.M. Bofill, J. Comput. Chem., 15 (1994) 1–11.
80 H.B. Schlegel, in: J. Bertrán, I.G. Csizmadia (Eds.), New theoretical concepts for understanding organic reactions, Kluwer, Dordrecht, 1989, pp. 33–53.
81 E. Besalu and J.M. Bofill, Theor. Chem. Acc., 100 (1998) 265–274.
82 J.M. Anglada and J.M. Bofill, Int. J. Quantum Chem., 62 (1997) 153–165.
83 P. Culot, G. Dive, V.H. Nguyen and J.M. Ghuysen, Theor. Chim. Acta, 82 (1992) 189–205.
84 A. Banerjee, N. Adams, J. Simons and R. Shepard, J. Phys. Chem., 89 (1985) 52–57.

85 T. Helgaker, Chem. Phys. Lett., 182 (1991) 503–510.
86 H.B. Schlegel, J. Comput. Chem., 3 (1982) 214–218.
87 J. Nocedal, Math. Comput., 35 (1980) 773–782.
88 D.C. Liu and J. Nocedal, Math. Program., 45 (1989) 503–528.
89 J.M. Anglada, E. Besalu, J.M. Bofill and J. Rubio, J. Math. Chem., 25 (1999) 85–92.
90 T.H. Fischer and J. Almlof, J. Phys. Chem., 96 (1992) 9768–9774.
91 P. Pulay, J. Comput. Chem., 3 (1982) 556–560.
92 P. Pulay, Chem. Phys. Lett., 73 (1980) 393–398.
93 P. Csaszar and P. Pulay, J. Mol. Struct., 114 (1984) 31–34.
94 Ö. Farkas, PhD (Csc) thesis, Eötvös Loránd University and Hungarian Academy of Sciences, Budapest, 1995.
95 O. Farkas and H.B. Schlegel, Phys. Chem. Chem. Phys., 4 (2002) 11–15.
96 O. Farkas and H.B. Schlegel, J. Mol. Struct. (THEOCHEM), 666 (2003) 31–39.
97 J. Gao, in Encyclopedia of computational chemistry, P.v.R. Schleyer, N.L. Allinger, T. Clark, J. Gasteiger, P.A. Kollman, H.F. Schaefer III, and P.R. Schreiner, (Eds.), Wiley, Chichester, 1998, pp. 1257–1263.
98 J. Gao, in: K.B. Lipkowitz, D.B. Boyd (Eds.), Reviews in computational chemistry, VCH, New York, 1996, pp. 119–185.
99 R.D.J. Froese and K. Morokuma, in Encyclopedia of computational chemistry, P.v.R. Schleyer, N.L. Allinger, T. Clark, J. Gasteiger, P.A. Kollman, H.F. Schaefer III, and P.R. Schreiner, (Eds.), Wiley, Chichester, 1998, pp. 1244–57.
100 K.M. Merz and R.V. Stanton, in Encyclopedia of computational chemistry, P.v.R. Schleyer, N.L. Allinger, T. Clark, J. Gasteiger, P.A. Kollman, H.F. Schaefer III and P.R. Schreiner, (Eds.), Wiley, Chichester, 1998, pp. 2330–2343.
101 J. Tomasi and C.S. Pomelli, in Encyclopedia of computational chemistry, P.v.R. Schleyer, N.L. Allinger, T. Clark, J. Gasteiger, P.A. Kollman, H.F. Schaefer III and P.R. Schreiner, (Eds.), Wiley, Chichester, 1998, pp. 2343–2350.
102 M.F. Ruiz-López and J.L. Rivail, in Encyclopedia of computational chemistry, P.v.R. Schleyer, N.L. Allinger, T. Clark, J. Gasteiger, P.A. Kollman, H.F. Schaefer III and P.R. Schreiner, (Eds.), Wiley, Chichester, 1998, pp. 437–48.
103 G. Monard and K.M. Merz, Acc. Chem. Res., 32 (1999) 904–911.
104 T.Z. Mordasini and W. Thiel, Chimia, 52 (1998) 288–291.
105 M.J. Field, P.A. Bash and M. Karplus, J. Comput. Chem., 11 (1990) 700–733.
106 U.C. Singh and P.A. Kollman, J. Comput. Chem., 7 (1986) 718–730.
107 A. Warshel and M. Levitt, J. Mol. Biol., 103 (1976) 227–249.
108 M. Svensson, S. Humbel, R.D.J. Froese, T. Matsubara, S. Sieber and K. Morokuma, J. Phys. Chem., 100 (1996) 19357–19363.
109 T. Vreven, B. Mennucci, C.O. da Silva, K. Morokuma and J. Tomasi, J. Chem. Phys., 115 (2001) 62–72.
110 S. Dapprich, I. Komaromi, K.S. Byun, K. Morokuma and M.J. Frisch, J. Mol. Struct. (THEOCHEM), 462 (1999) 1–21.
111 A.J. Turner, V. Moliner and I.H. Williams, Phys. Chem. Chem. Phys., 1 (1999) 1323–1331.
112 T. Vreven, K. Morokuma, O. Farkas, H.B. Schlegel and M.J. Frisch, J. Comp. Chem., 24 (2003) 760–769.
113 M. Sierka and J. Sauer, J. Chem. Phys., 112 (2000) 6983–6996.
114 Y.K. Zhang, H.Y. Liu and W.T. Yang, J. Chem. Phys., 112 (2000) 3483–3492.
115 D.R. Yarkony, Rev. Mod. Phys., 68 (1996) 985–1013.
116 D.R. Yarkony, Acc. Chem. Res., 31 (1998) 511–518.
117 D.R. Yarkony, J. Phys. Chem. A, 105 (2001) 6277–6293.
118 D.R. Yarkony, J. Chem. Phys., 92 (1990) 2457–2463.
119 D.R. Yarkony, J. Phys. Chem., 97 (1993) 4407–4412.
120 D.R. Yarkony, J. Phys. Chem. A, 108 (2004) 3200–3205.
121 M.R. Manaa and D.R. Yarkony, J. Chem. Phys., 99 (1993) 5251–5256.
122 J.M. Anglada and J.M. Bofill, J. Comput. Chem., 18 (1997) 992–1003.

123 M.J. Bearpark, M.A. Robb and H.B. Schlegel, Chem. Phys. Lett., 223 (1994) 269–274.
124 M.J. Frisch, G.W. Trucks, H.B. Schlegel, G.E. Scuseria, M.A. Robb, J.R. Cheeseman, J.A.M. Jr., T. Vreven, K.N. Kudin, J.C. Burant, J.M. Millam, S.S. Iyengar, J. Tomasi, V. Barone, B. Mennucci, M. Cossi, G. Scalmani, N. Rega, G.A. Petersson, H. Nakatsuji, M. Hada, M. Ehara, K. Toyota, R. Fukuda, J. Hasegawa, M. Ishida, T. Nakajima, Y. Honda, O. Kitao, H. Nakai, M. Klene, X. Li, J.E. Knox, H.P. Hratchian, J.B. Cross, C. Adamo, J. Jaramillo, R. Gomperts, R.E. Stratmann, O. Yazyev, A.J. Austin, R. Cammi, C. Pomelli, J.W. Ochterski, P.Y. Ayala, K. Morokuma, G.A. Voth, P. Salvador, J.J. Dannenberg, V.G. Zakrzewski, S. Dapprich, A.D. Daniels, M.C. Strain, O. Farkas, D.K. Malick, A.D. Rabuck, K. Raghavachari, J.B. Foresman, J.V. Ortiz, Q. Cui, A.G. Baboul, S. Clifford, J. Cioslowski, B.B. Stefanov, G. Liu, A. Liashenko, P. Piskorz, I. Komaromi, R.L. Martin, D.J. Fox, T. Keith, M.A. Al-Laham, C.Y. Peng, A. Nanayakkara, M. Challacombe, P.M.W. Gill, B. Johnson, W. Chen, M.W. Wong, C. Gonzalez and J.A. Pople, GAUSSIAN 03. Gaussian, Inc., Pittsburgh, PA, 2003.
125 H.B. Schlegel, Int. J. Quantum Chem. Quantum Chem. Symp., 24 (1992) 243–252.
126 When using programs written in FORTRAN these values are generally reported as infinity, 'inf', or not a number, 'nan', in the output.
127 H.B. Schlegel, Theor. Chim. Acta, 66 (1984) 333–340.
128 H.B. Schlegel, J. Comput. Chem., 24 (2003) 1514–1527.
129 J.M. Anglada and J.M. Bofill, J. Comput. Chem., 19 (1998) 349–362.
130 J.M. Bofill, Chem. Phys. Lett., 260 (1996) 359–364.
131 J.M. Bofill and M. Comajuan, J. Comput. Chem., 16 (1995) 1326–1338.
132 J. Simons, P. Jorgensen, H. Taylor and J. Ozment, J. Phys. Chem., 87 (1983) 2745–2753.
133 J.M. Bofill and J.M. Anglada, Theor. Chem. Acc., 105 (2001) 463–472.
134 J. Baker, J. Comput. Chem., 7 (1986) 385–395.
135 C.J. Cerjan and W.H. Miller, J. Chem. Phys., 75 (1981) 2800–2806.
136 J. Nichols, H. Taylor, P. Schmidt and J. Simons, J. Chem. Phys., 92 (1990) 340–346.
137 J. Pancir, Collect. Czech. Chem. Commun., 40 (1975) 1112–1118.
138 C.Y. Peng and H.B. Schlegel, Isr. J. Chem., 33 (1993) 449–454.
139 T. Halgren and W.N. Lipscomb, Chem. Phys. Lett., 49 (1977) 225–232.
140 F. Jensen, J. Chem. Phys., 119 (2003) 8804–8808.
141 F. Jensen and P.O. Norrby, Theor. Chem. Acc., 109 (2003) 1–7.
142 F. Jensen, J. Comput. Chem., 15 (1994) 1199–1216.
143 K. Mueller and L.D. Brown, Theor. Chim. Acta, 53 (1979) 75–93.
144 M.J.S. Dewar, E.F. Healy and J.J.P. Stewart, J. Chem. Soc. Faraday Trans. II, 80 (1984) 227–233.
145 C. Cardenas-Lailhacar and M.C. Zerner, Int. J. Quantum Chem., 55 (1995) 429–439.
146 I.V. Ionova and E.A. Carter, J. Chem. Phys., 98 (1993) 6377–6386.
147 I.V. Ionova and E.A. Carter, J. Chem. Phys., 103 (1995) 5437–5441.
148 S. Bell and J.S. Crighton, J. Chem. Phys., 80 (1984) 2464–2475.
149 A. Jensen, Theor. Chim. Acta, 63 (1983) 269–290.
150 J.M. Anglada, E. Besalu, J.M. Bofill and R. Crehuet, J. Comput. Chem., 20 (1999) 1112–1129.
151 F. Bernardi, J.J.W. McDouall and M.A. Robb, J. Comput. Chem., 8 (1987) 296–306.
152 J.J.W. McDouall, M.A. Robb and F. Bernardi, Chem. Phys. Lett., 129 (1986) 595–602.
153 I.H. Williams and G.M. Maggiora, J. Mol. Struct. (THEOCHEM), 6 (1982) 365–378.
154 M.J. Rothman and L.L. Lohr, Chem. Phys. Lett., 70 (1980) 405–409.
155 P. Scharfenberg, Chem. Phys. Lett., 79 (1981) 115–117.
156 W. Quapp, Chem. Phys. Lett., 253 (1996) 286–292.
157 W. Quapp, M. Hirsch and D. Heidrich, Theor. Chem. Acc., 105 (2000) 145–155.
158 W. Quapp, M. Hirsch, O. Imig and D. Heidrich, J. Comput. Chem., 19 (1998) 1087–1100.
159 W. Quapp, Comput. Math. Appl., 41 (2001) 407–414.
160 M. Hirsch and W. Quapp, J. Comput. Chem., 23 (2002) 887–894.
161 R. Crehuet, J.M. Bofill and J.M. Anglada, Theor. Chem. Acc., 107 (2002) 130–139.
162 K. Fukui, Acc. Chem. Res., 14 (1981) 363–368.
163 L.R. Pratt, J. Chem. Phys., 85 (1986) 5045–5048.
164 R. Elber and M. Karplus, Chem. Phys. Lett., 139 (1987) 375–380.

165 G. Henkelman and H. Jónsson, J. Chem. Phys., 113 (2000) 9978–9985.
166 P.Y. Ayala and H.B. Schlegel, J. Chem. Phys., 107 (1997) 375–384.
167 B. Peters, A. Heyden, A.T. Bell and A. Chakraborty, J. Chem. Phys., 120 (2004) 7877–7886.
168 C. Choi and R. Elber, J. Chem. Phys., 94 (1991) 751–760.
169 R. Czerminski and R. Elber, Int. J. Quantum Chem., (1990) 167–186.
170 R. Czerminski and R. Elber, J. Chem. Phys., 92 (1990) 5580–5601.
171 A. Ulitsky and R. Elber, J. Chem. Phys., 92 (1990) 1510–1511.
172 O.S. Smart, Chem. Phys. Lett., 222 (1994) 503–512.
173 E.M. Sevick, A.T. Bell and D.N. Theodorou, J. Chem. Phys., 98 (1993) 3196–3212.
174 R.E. Gillilan and K.R. Wilson, J. Chem. Phys., 97 (1992) 1757–1772.
175 T.L. Beck, J.D. Doll and D.L. Freeman, J. Chem. Phys., 90 (1989) 3181–3191.
176 G. Henkelman, B.P. Uberuaga and H. Jonsson, J. Chem. Phys., 113 (2000) 9901–9904.
177 C. Gonzalez and H.B. Schlegel, J. Chem. Phys., 90 (1989) 2154–2161.
178 C. Gonzalez and H.B. Schlegel, J. Phys. Chem., 94 (1990) 5523–5527.
179 H. Jónsson, G. Mills and W. Jacobsen, in: B.J. Berne, G. Cicotti, D.F. Coker (Eds.), Classical and quantum dynamics in condensed phase simulations, World Scientific, Singapore, 1998, p. 385.
180 P. Maragakis, S.A. Andreev, Y. Brumer, D.R. Reichman and E. Kaxiras, J. Chem. Phys., 117 (2002) 4651–4658.
181 D.J. Wales, Mol. Phys., 100 (2002) 3285–3305.
182 S.A. Trygubenko and D.J. Wales, J. Chem. Phys., 120 (2004) 2082–2094.
183 J.W. Chu, B.L. Trout and B.R. Brooks, J. Chem. Phys., 119 (2003) 12708–12717.
184 H.L. Woodcock, M. Hodoscek, P. Sherwood, Y.S. Lee, H.F. Schaefer and B.R. Brooks, Theor. Chem. Acc., 109 (2003) 140–148.
185 Y. Abashkin and N. Russo, J. Chem. Phys., 100 (1994) 4477–4483.
186 E. Weinan, W.Q. Ren and E. Vanden-Eijnden, Phys. Rev. B, 66 (2002).
187 B.C. Garrett and D.G. Truhlar, J. Phys. Chem., 83 (1979) 1079–1112.
188 A.D. Isaacson and D.G. Truhlar, J. Phys., 76 (1982) 1380–1381.
189 I. Shavitt, J. Chem. Phys., 49 (1968) 4048–4056.
190 D.G. Truhlar and A. Kuppermann, J. Am. Chem. Soc., 93 (1971) 1840–1851.
191 D.G. Truhlar and A. Kuppermann, J. Chem. Phys., 56 (1972) 2232–2252.
192 M.V. Basilevsky and A.G. Shamov, Chem. Phys., 60 (1981) 347–358.
193 D.K. Hoffman, R.S. Nord and K. Ruedenberg, Theor. Chim. Acta, 69 (1986) 265–279.
194 P. Jorgensen, H.J.A. Jensen and T. Helgaker, Theor. Chim. Acta, 73 (1988) 55–65.
195 H.B. Schlegel, Theor. Chim. Acta, 83 (1992) 15–20.
196 J.Q. Sun and K. Ruedenberg, J. Chem. Phys., 98 (1993) 9707–9714.
197 P.G. Bolhuis, C. Dellago and D. Chandler, Faraday Discuss., (1998) 421–436.
198 P.G. Bolhuis, C. Dellago, P.L. Geissler and D. Chandler, J. Phys.-Condens. Matter, 12 (2000) A147–A152.
199 B.R. Brooks, Y.S. Lee and T.E. Cheatham, Abstr. Pap. Am. Chem. Soc., 222 (2001) 63-COMP.
200 G.E. Crooks and D. Chandler, Phys. Rev. E, 6402 (2001) 026109–026112.
201 C. Dellago, P.G. Bolhuis and D. Chandler, J. Chem. Phys., 110 (1999) 6617–6625.
202 C. Dellago, P.G. Bolhuis, F.S. Csajka and D. Chandler, J. Chem. Phys., 108 (1998) 1964–1977.
203 A. Michalak and T. Ziegler, J. Phys. Chem. A, 105 (2001) 4333–4343.
204 L. Rosso, P. Minary, Z.W. Zhu and M.E. Tuckerman, J. Chem. Phys., 116 (2002) 4389–4402.
205 L. Rosso and M.E. Tuckerman, Mol. Simul., 28 (2002) 91–112.
206 C.W. Gear, Numerical initial value problems in ordinary differential equations, Prentice-Hall, Englewood Cliffs, NJ, 1971.
207 K.K. Baldridge, M.S. Gordon, R. Steckler and D.G. Truhlar, J. Phys. Chem., 93 (1989) 5107–5119.
208 B.C. Garrett, M.J. Redmon, R. Steckler, D.G. Truhlar, K.K. Baldridge, D. Bartol, M.W. Schidt and M.S. Gordon, J. Phys. Chem., 92 (1988) 1476–1488.
209 C. Gonzalez and H.B. Schlegel, J. Chem. Phys., 95 (1991) 5853 5860.
210 H.P. Hratchian and H.B. Schlegel, J. Chem. Phys., 120 (2004) 9918–9924.
211 H.P. Hratchian and H.B. Schlegel, J. Chem. Theory Comp. 1 (2004) 61–69.

212 K. Ishida, K. Morokuma and A. Komornicki, J. Chem. Phys., 66 (1977) 2153–2156.
213 K. Müller and L.D. Brown, Theor. Chim. Acta, 53 (1979) 75–93.
214 M. Page, C. Doubleday and J.W. McIver, J. Chem. Phys., 93 (1990) 5634–5642.
215 M. Page and J.M. McIver, J. Chem. Phys., 88 (1988) 922–935.
216 M.W. Schmidt, M.S. Gordon and M. Dupuis, J. Am. Chem. Soc., 107 (1985) 2585–2589.
217 J.Q. Sun and K. Ruedenberg, J. Chem. Phys., 99 (1993) 5269–5275.
218 M.S. Gordon, G. Chaban and T. Taketsugu, J. Phys. Chem., 100 (1996) 11512–11525.
219 H.P. Hratchian and H.B. Schlegel, J. Phys. Chem. A, 106 (2002) 165–169.
220 S.A. Maluendes and M.J. Dupuis, J. Chem. Phys., 93 (1990) 5902–5911.
221 J.J.P. Stewart, L.P. Davis and L.W. Burggraf, J. Comput. Chem., 8 (1987) 1117–1123.
222 V. Bakken, J.M. Millam and H.B. Schlegel, J. Chem. Phys., 111 (1999) 8773–8777.
223 J.M. Millam, V. Bakken, W. Chen, W.L. Hase and H.B. Schlegel, J. Chem. Phys., 111 (1999) 3800–3805.
224 R. Bulirsch and J. Stoer, Num. Math., 6 (1964) 413–427.
225 R. Bulirsch and J. Stoer, Num. Math., 8 (1966) 1–13.
226 R. Bulirsch and J. Stoer, Num. Math., 8 (1966) 93–104.
227 W.H. Press, Numerical recipes in FORTRAN 77: The art of scientific computing, Cambridge University Press, Cambridge, 1996.
228 R.P.A. Bettens and M.A. Collins, J. Chem. Phys., 111 (1999) 816–826.
229 M.A. Collins, Theor. Chem. Acc., 108 (2002) 313–324.
230 J. Ischtwan and M.A. Collins, J. Chem. Phys., 100 (1994) 8080–8088.
231 K.C. Thompson, M.J.T. Jordan and M.A. Collins, J. Chem. Phys., 108 (1998) 564–578.
232 F. Eckert and H.J. Werner, Theor. Chem. Acc., 100 (1998) 21–30.
233 V.S. Melissas, D.G. Truhlar and B.C. Garrett, J. Chem. Phys., 96 (1992) 5758–5772.
234 A.G. Baboul and H.B. Schlegel, J. Chem. Phys., 107 (1997) 9413–9417.
235 E.B. Wilson, J.C. Decius and P.C. Cross, The theory of infrared and Raman vibrational spectra, McGraw-Hill, New York, 1955.
236 P. Valtazanos and K. Ruedenberg, Theor. Chim. Acta, 69 (1986) 281–307.
237 J. Baker and P.M.W. Gill, J. Comput. Chem., 9 (1988) 465–475.
238 V. Bakken, D. Danovich, S. Shaik and H.B. Schlegel, J. Am. Chem. Soc., 123 (2001) 130–134.
239 M.V. Basilevsky, Theor. Chim. Acta, 72 (1987) 63–67.
240 Y. Kumeda and T. Taketsugu, J. Chem. Phys., 113 (2000) 477–484.
241 B. Lasorne, G. Dive, D. Lauvergnat and M. Desouter-Lecomte, J. Chem. Phys., 118 (2003) 5831–5840.
242 B. Peters, W.Z. Liang, A.T. Bell and A. Chakraborty, J. Chem. Phys., 118 (2003) 9533–9541.
243 W. Quapp, J. Theor. Comput. Chem., 2 (2003) 385–417.
244 W. Quapp, J. Comput. Chem., 25 (2004) 1277–1285.
245 W. Quapp, J. Mol. Struct., 695 (2004) 95–101.
246 W. Quapp, M. Hirsch and D. Heidrich, Theor. Chem. Acc., 100 (1998) 285–299.
247 M.N. Ramquet, G. Dive and D. Dehareng, J. Chem. Phys., 112 (2000) 4923–4934.
248 T. Taketsugu and T. Hirano, J. Mol. Struct. (THEOCHEM), 116 (1994) 169–176.
249 T. Taketsugu and Y. Kumeda, J. Chem. Phys., 114 (2001) 6973–6982.
250 T. Taketsugu, N. Tajima and K. Hirao, J. Chem. Phys., 105 (1996) 1933–1939.
251 T. Yanai, T. Taketsugu and K. Hirao, J. Chem. Phys., 107 (1997) 1137–1146.
252 A. Andersen and E.A. Carter, J. Phys. Chem. A, 107 (2003) 9463–9478.
253 A. Andersen and E.A. Carter, Isr. J. Chem., 42 (2002) 245–260.